Document downloaded from:

http://hdl.handle.net/10251/192510

This paper must be cited as:

Lerida-Viso, A.; Estepa-Fernández, A.; Morella-Aucejo, Á.; Lozano-Torres, B.; Alfonso, M.; Blandez, JF.; Bisbal, V.... (2022). Pharmacological senolysis reduces doxorubicin-induced cardiotoxicity and improves cardiac function in mice. Pharmacological Research. 183:1-16. https://doi.org/10.1016/j.phrs.2022.106356

The final publication is available at

https://doi.org/10.1016/j.phrs.2022.106356

Copyright Elsevier

Additional Information

Pharmacological senolysis reduces doxorubicin-induced cardiotoxicity and improves cardiac function in mice

Araceli Lérida-Viso[1,2,3,4], Alejandra Estepa- Fernández[2,3,4], Ángela Morellá-Aucejo[2,3,4], Beatriz Lozano-Torres[2,3,4], María Alfonso[2], Juan F. Blandez[1,2,4], Viviana Bisbal[5], Pilar Sepúlveda[6,7], Alba García-Fernández[2,3,4,*], Mar Orzáez[3,5,*], Ramón Martínez-Máñez[1,2,3,4,*].

1 Unidad Mixta de Investigación en Nanomedicina y Sensores. Universitat Politècnica de València (UPV)- Instituto de Investigación Sanitaria La Fe (IIS La Fe).
Av. Fernando Abril Martorell 106, Valencia 46026, Spain

2 Instituto Interuniversitario de Investigación de Reconocimiento Molecular y Desarrollo Tecnológico (IDM). Universitat Politècnica de València.
Camino de Vera, s/n, Valencia 46022, Spain

3 Unidad Mixta UPV-CIPF de Investigación en Mecanismos de Enfermedades y Nanomedicina. Universitat Politècnica de València-Centro de Investigación Príncipe Felipe.
C/ Eduardo Primo Yúfera 3, Valencia 46012, Spain

4 CIBER de Bioingeniería Biomateriales y Nanomedicina (CIBER-BBN).

5 Centro de Investigación Príncipe Felipe.
C/ Eduardo Primo Yúfera 3, Valencia 46012, Spain.

6 Regenerative Medicine and Heart Transplantation Unit. Instituto de Investigación Sanitaria La Fe. Av. Fernando Abril Martorell 106, Valencia 46026, Spain

7 CIBER de Enfermedades Cardiovasculares (CIBERCV).

E-mail: algarfe4@etsia.upv.es; morzaez@cipf.es; rmaez@qim.upv.es

Graphical Abstract

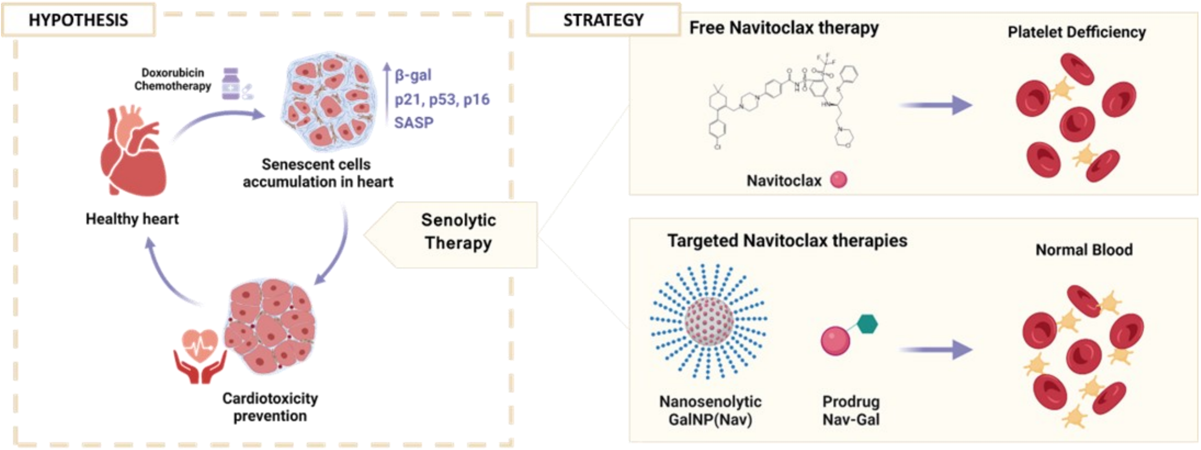

Keywords: Doxorubicin, cardiac senescence, senolytic, navitoclax, nanoparticles, prodrug

Abstract: Many anticancer agents used in clinics induce premature senescence in healthy tissues generating accelerated aging processes and adverse side-effects in patients. Cardiotoxicity is a well-known limiting factor of anticancer treatment with doxorubicin (DOX), a very effective anthracycline widely used as antitumoral therapy in clinical practice, that leads to long-term morbidity and mortality. DOX exposure severely affects the population of cardiac cells in both mice and human hearts by inducing premature senescence, which may represent the molecular basis of DOX-induced cardiomyopathy. Here, we demonstrate that senescence induction in the heart contributes to impaired cardiac function in mice upon DOX treatment. Concomitant elimination of senescent cells with the senolytic Navitoclax in different formulations produces a significant decrease in senescence and cardiotoxicity markers together with the restoration of the cardiac function in mice followed by echocardiography. These results evidence the potential clinical use of senolytic therapies to alleviate cardiotoxicities induced in chemotherapy-treated patients.

1. Introduction

Cellular senescence is a mechanism of cell cycle arrest in response to different stimuli which can be related either to normal physiological or pathological conditions [1]. The accumulation of senescent cells contributes to age-related disorders and negatively affects the regenerative capacity of organs and tissues [2]. The presence of senescent cells in the cardiovascular system, including the heart, links with diverse cardiac disorders, such as heart failure and atherosclerotic diseases [3,4]. In addition, the presence of senescent cardiomyocytes has been described during physiological aging in mice and humans, contributing to the progression of cardiac dysfunction [5,6]. Besides many chemotherapy drugs promote therapy-induced senescence (TIS) either as the therapeutic mechanism of action or as a side-effect [7]. This is the case of Doxorubicin (DOX), a very effective anthracycline widely used as antitumoral therapy in clinical practice [8]. One of the main side-effects of DOX is the induction of adverse cardiotoxicity, which can appear in an acute manner or many years after drug administration to cancer patients, representing an important public health concern [8–10]. Despite the mechanism underlying DOX-induced cardiotoxicity remains controversial, some studies indicate that DOX induces significant damage to cardiomyocyte cells that eventually leads to premature senescence [11,12]. Moreover, endothelial cells and fibroblast-like cells in the heart also achieve a senescence phenotype in DOX-treated mice [7]. Besides, it has been reported that DOX treatment in humans and murine models produces an accumulation of senescent cardiac progenitor cells (CPCs) in the heart that correlates with a decline in the regeneration capacity thus causing long-term toxicity in patients [13,14].

From another point of view, the selective elimination of senescent cells, known as senolysis, has been validated as a novel therapy to blunt the deleterious and pro-aging associated effects in different disease models and enhance health- and lifespan in old mice [15–17]. Concerning the heart, the genetic depletion of accumulated p16Ink4a-positive senescent cells delays the acquisition of aged phenotypes in the heart in an aging mouse model [18]. Besides, Hoshino *et al.*, demonstrated that inhibition of cytosolic p53 may ameliorate heart failure and symptoms of cardiac aging after DOX treatment *in vivo* [19]. These genetically engineered mouse models evidenced new targets to improve the translation of new therapeutic strategies.

In an attempt to move toward practical applications, researchers have identified pharmacological compounds that preferentially kill senescent cells, commonly known as senolytics [20,21]. Among them, Dasatinib and Quercetin (D+Q) administered in combination significantly ameliorate age-related heart dysfunction improving left ventricular ejection fraction and fractional shortening [22]. Furthermore, D+Q led to the activation of resident CPCs and increased the number of proliferative cardiomyocytes in old mice, restoring the regenerative capacity of the heart [23]. However, the clinical use of these senolytic treatments correlates with side-effects in patients [24]. Another relevant senolytic drug is the anticancer agent Navitoclax (also known as ABT-263), a potent inhibitor of the anti-apoptotic Bcl-2 family, whose expression is highly increased in senescent cells [22]. Navitoclax delays age-related pathologies in cardiac tissue through the elimination of senescent cardiomyocytes and attenuated cardiac hypertrophy and fibrosis in aged mice [6]. Furthermore, its use ameliorated myocardial remodeling, diastolic function, improved survival rate before myocardial infarction [25], and promoted recovery after ischemia-reperfusion [26]. Nevertheless, the clinical use of Navitoclax is hampered due to its associated hematological toxicity, causing severe thrombocytopenia and neutropenia [27].

In this scenario, the elimination of senescent cells could have a therapeutic effect as a protective intervention to combat DOX-induced senescence during chemotherapy regimens. However, in this context, no studies have been carried out on the use of pharmacological senolytics for the elimination of senescent cells in cardiotoxicity induced by chemotherapy models and on the potential therapeutic effects of their elimination. Based on the above, we report herein that DOX treatment induces heart senescence and expression of cardiotoxicity markers in adult mice. Concomitant administration of Navitoclax in different formulations is effective in eliminating senescent cells in the heart, which correlates with the recovery of cardiac function in a mouse model of doxorubicin-induced cardiotoxicity. Free Navitoclax, Navitoclax encapsulated in mesoporous silica nanoparticles and capped with a hexagalactosaccharide (galactan) (**GalNP(Nav)**) and a prodrug obtained by galacto-conjugation with Navitoclax (**Nav-Gal**) are used. Overall, we provide evidence of the use of senolytics to reduce doxorubicin-associated cardiotoxicity, which might help to overcome the clinical limitations of current chemotherapy treatments.

2. Results

2.1. DOX induces cell cycle arrest and senescence in HL-1 cardiac myocyte cell line

To validate the use of the proposed senolytic therapeutical strategies in cardiac pathologies associated with DOX, we first carried out *in vitro* studies. As adult mammalian cardiomyocytes are predominantly post-mitotic and cannot be expanded *in vitro*, we selected the proliferating HL-1 cardiac myocyte cell line to validate different therapeutical approaches [28]. These cells, even immortalized, maintain a cardiac-specific phenotype and have been previously used as experimental model for cardiomyocyte-induced senescence [29].

First, the induction of senescence by DOX in the HL- 1 cardiac myocyte cell line was evaluated. We found that treatment with DOX 100 nM for 72h was enough to induce senescence in HL-1 cells (**Figure 1A-F)** without causing cell death (**Figure S1A**). DOX-treated HL-1 cells showed increased lysosomal β-galactosidase activity, a typical marker of senescence activation, evidenced by the increment in blue-stained cells observed in X-Gal staining assays *versus* untreated cells (**Figure 1A**) [30]. In line with these results, flow cytometry studies using the lipophilic ß-galactosidase substrate 5-dodecanoylaminofluorescein di-β-D-galactopyranoside (C_{12}FDG) confirmed the accumulation of senescent population in DOX-treated HL-1 cardiomyocytes (3-fold) compared to non-treated cells (**Figure 1B).** Moreover, cell cycle analyses by flow cytometry after DOX treatment for 72h showed that DOX-induced accumulation of cells in the G2/M-phase, a hallmark of the cell cycle effect of DOX treatment [31] (**Figure 1C**), and the time-lapse imaging confirmed the suppression of proliferation in HL-1 cells by 100 nM DOX (**Figure 1D**). Additionally, the proliferation arrest assay by crystal violet staining after one week in culture and the immunostaining of the Ki67 proliferation marker demonstrated the stop of cellular proliferation for DOX-treated HL-1 cells confirming cell cycle arrest (**Figure S1C-D**).

It is now well recognized that most stressors that induce cellular senescence activate either or both the p53/p21 or p16Ink4a/retinoblastoma (Rb) protein pathways to prevent entry into the cell cycle [32,33]. Hypo-phosphorylation in retinoblastoma (Rb) protein and upregulation of p53 and p21 were observed in extracts of DOX-treated HL-1 cells, as is expected for a senescent phenotype (**Figure 1E.** Original images in **Figure S2A).** We also demonstrated the induction of β-galactosidase (β-gal) protein expression by western blot. In our regard, the importance of β-galactosidase up-expression is essential for validating our targeted strategies, as the proper performance of both, nanoparticles (**GalNP(Nav)**) and the prodrug (**Nav-Gal**) depends on this activity (*vide infra*). The up-expression of *p21* and *p53* (**Figure 1F)** and the SASP markers *Cxcl1* and *IL6* (**Figure S1B)** were also confirmed at mRNA levels in HL-1 cells in response to DOX exposure. Thus, cell cycle exit, and senescence after DOX exposure are accompanied by the activation of the cell cycle inhibitors p53/p21 and hypo-phosphorylation in retinoblastoma (Rb) protein, β-gal induction, and SASP expression.

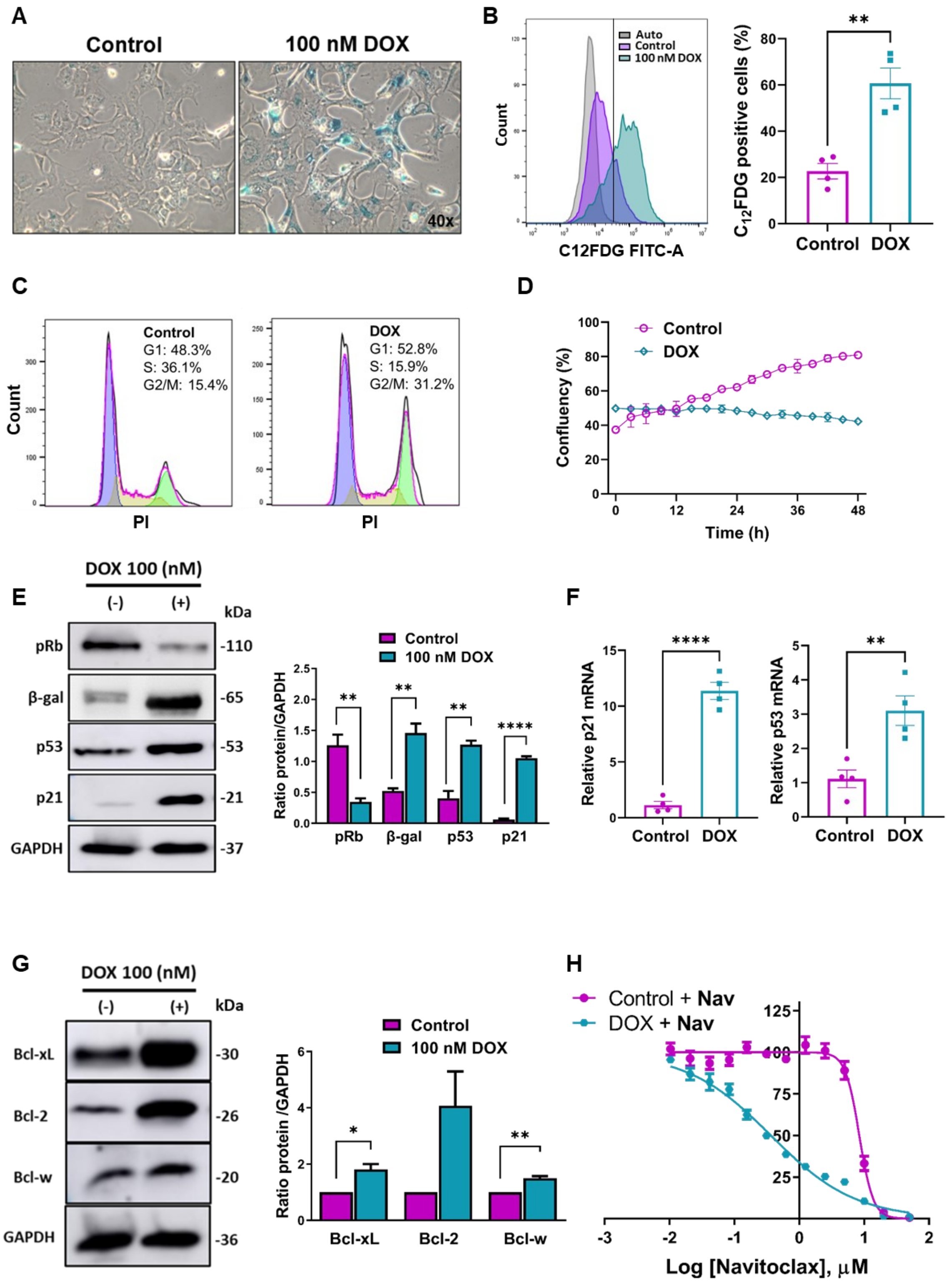

Figure 1. Doxorubicin (DOX) treatment induces cellular senescence in HL-1 cardiac myocytes cells and Navitoclax exhibits senolytic activity in senescent cardiac myocytes. **(A)** Representative bright-field images of SA-β-gal staining of control and 100 nM DOX-treated HL-1 cells. Blue staining confirms high β-galactosidase activity at pH 6 upon DOX treatment. **(B)** Histogram and percentage of C_{12}FDG positive cells indicate β-galactosidase

activity in control and DOX-treated cells by flow cytometry. Values are expressed as mean ± SEM and statistical significance was assessed by the two-tailed Student's t-test: **p<0.01 (n=4). (**C**) Cell cycle distribution was measured using flow cytometry. Propidium iodide (PI) staining of control and 100 nM DOX-treated HL-1 cells. DOX-treated cells accumulate in cell cycle G2/M after 3 days of treatment. (**D**) Graphs represent confluency (%) of HL-1 control and DOX-treated cells followed by time-lapse imaging, showing suppression of proliferation in HL-1 cells by 100 nM DOX. **(E)** (Left) Representative western blot analysis showing the decrease in phospho-retinoblastoma (pRb) expression (110 kDa) and the increment in β-galactosidase (65 kDa), p53 (53 kDa), and p21 (21 kDa) protein expression for DOX-treated HL-1 cells. GAPDH (37 kDa) was included as a loading control. (Right) Quantification of ratio protein expression versus internal reference (GAPDH) in control and DOX-treated cells. Values are expressed as mean ± SEM and statistical significance was assessed by the two-tailed Student's t-test: *p<0.05; **p<0.01; ****p<0.0001 (n≥3). **(F)** mRNA expression levels of the senescent makers *p21* and *p53* in HL-1 control and DOX-treated cells. *Actb* was used for input normalization. Bars represent the mean ± SEM and statistical significance was assessed by the two-tailed Student's t-test: **p<0.01 (n≥3). **(G)** (Left) Representative western blot analysis expression of Bcl-2 family protein profile. Increased expression of anti-apoptotic proteins Bcl-xL (30 kDa), Bcl-2 (26 kDa), and Bcl-w (20 kDa) was found in DOX treated HL-1 cells. GAPDH (37 kDa) determination was included as a loading control. (Right) Quantification of ratio anti-apoptotic protein expression versus internal control (GAPDH) in control and DOX-treated cells. Values are expressed as mean ± SEM and statistical significance was assessed by the two-tailed Student's t-test:*p<0.05; **p<0.01 (n≥3). (**H**) IC50 curves obtained with increasing concentrations of free Navitoclax (0.01 to 50 μM) for control and DOX-treated cells measured after 48h of treatment by luminescent ATP detection. Values are expressed as mean ± SEM (n=8).

2.2. Navitoclax in different formulations exhibits senolytic activity in senescent cardiac myocytes

Once the induction of cellular senescence in the HL-1 cardiac myocyte cell line upon DOX treatment was demonstrated, we evaluated the effectiveness of the senolytic Navitoclax *in vitro.* As Navitoclax is an inhibitor of the anti-apoptotic proteins Bcl-2, Bcl-xL, and Bcl-w, we first analyzed changes in Bcl-2 family proteins expression upon DOX treatment in HL-1 cardiomyocytes. We corroborated the upregulation of these anti-apoptotic proteins (**Figure 1G.** Original images in **Figure S2B**), as well as the pro-apoptotic proteins Bim, Bok, and Bax that were also upregulated in senescent HL-1 cells (**Figure S1E.** Original images in **Figure S2B**). These results indicated dysregulation in apoptosis machinery after DOX exposure with high dependence on anti-apoptotic proteins for survival. Next, we treated control and senescent HL-1 cells with increasing concentrations of Navitoclax for 48h. Navitoclax exhibited senolytic activity by selectively inducing apoptosis on senescent HL-1 cells (**Figure 1H**). The IC50 value was calculated for both control (IC50 = 8.43 μM) and senescent cells (IC50 = 0.37 μM), resulting in a senolytic index of 23 (**Figure 3E**). Besides, we performed an X-gal staining including control and DOX-treated cells treated with Navitoclax (IC50 for senescent cells: 0.37μM) (**Figure S1F**). These results confirm Navitoclax treatment resulted in a reduction in the number of senescent cells but not control, which reinforces the role of Navitoclax as a senolytic therapy.

Considering our purpose to overcome the toxicity limitations of Navitoclax (e.g., hematological toxicities), we took advantage of the high lysosomal β-galactosidase (β-gal) activity present in senescent cells and encapsulate Navitoclax in mesoporous silica nanoparticles capped with a hexagalactosaccharide (galactan) to specifically target senescent cells and avoid cargo leakage. We have previously reported the senolytic potential of these nanoparticles in models of dyskeratosis congenita, chemotherapy-treated xenografts, pulmonary fibrosis, and endothelial-induced senescence [34–37]. The synthesis of the nanoparticles has been reported elsewhere [36]. Briefly, the mesoporous silica nanoparticles (MSNs) are loaded with indocyanine green (ICG, for tracking purposes), or Navitoclax (Nav, for treatment), and coated with galactan (solids **GalNP(ICG)** and **GalNP(Nav)**, respectively). When the galactan-gated nanodevices reach senescent cells, the lysosomal β-galactosidase activity induces the hydrolysis of the cap with the subsequent preferential cargo release into senescent cells (**Figure 2A**) [35]. To evaluate the biocompatibility of the mesoporous silica carrier in HL-1 cardiomyocytes, galactan-capped nanoparticles without cargo were also prepared (**GalNP**).

The synthesis of nanoparticles was carefully characterized by standard methods to assure their quality and reproducibility [34,36]. TEM (**Figure 2C)** and Powder X-ray diffraction studies **(Figure S3A**) confirmed the presence of the mesoporous structure of the starting nanoparticles as well as the spherical morphology and size of ca. 100 nm, which are maintained after the loading and functionalization processes. Starting MSNs exhibit a total specific surface area of 1228.80 $m^2 g^{-1}$ and a pore size of 3.18 nm (**Figure S3B, Table S1**). In contrast, data for functionalized nanoparticles **GalNP (Figure S3D),** and **GalNP(ICG)** (**Figure S3C**) showed substantial reduction of specific surface areas, which agrees with partially filled mesopores

(**Table S1**). Zeta potential was -27.1 mV for starting calcined MSNs which changed to -0.06 mV and 0.34 mV for final **GalNP(ICG)** and **GalNP(Nav)**, respectively (**Table S2**). Besides, the hydrodynamic diameter increased from 153.5 nm for the calcined MSNs to 244.5 nm and 284.8 nm for **GalNP(ICG)** and **GalNP(Nav)**, respectively (**Table S2**). In all cases, a single population distribution was observed in DLS for all solids suggesting no aggregation. From thermogravimetric and elemental analysis, the amounts of cargo (ICG or Nav) and galactan in final NPs were determined (**Table S3**). Controlled cargo release of **GalNP(Nav)** and **GalNP(ICG)**, was also confirmed by delivery studies in the absence and the presence of the enzyme β-galactosidase (**Figure 2D and S4B**). A clear cargo release was observed in the presence of the enzyme due to β-galactosidase-mediated hydrolysis of galactan and subsequent cargo release. In contrast, in the absence of the enzyme, a flat baseline was observed indicating that cargo remained in the NPs with no release.

HL-1 cell viability studies under increasing concentrations of **GalNP** (0-2 mg/ml, filtered) demonstrated cell survival up to 90% after 72h exposure, even at high concentrations (**Figure S4A**) confirming that the mesoporous silica carrier is not toxic. Besides, **GalNP(ICG)** was used to follow the cellular uptake of the nanoparticles by confocal microscopy and flow cytometry. After 4h of incubation, an increase in far-red fluorescence signal inside HL-1 senescent cells was observed, indicative of nanoparticle internalization and fluorophore delivery (**Figure 2E)**. In contrast, control cells showed a negligible emission under similar exposure. Flow cytometry studies also showed a significant fluorescence increase in **GalNP(ICG)-**treated senescent cells versus control cells (**Figure 2F).**

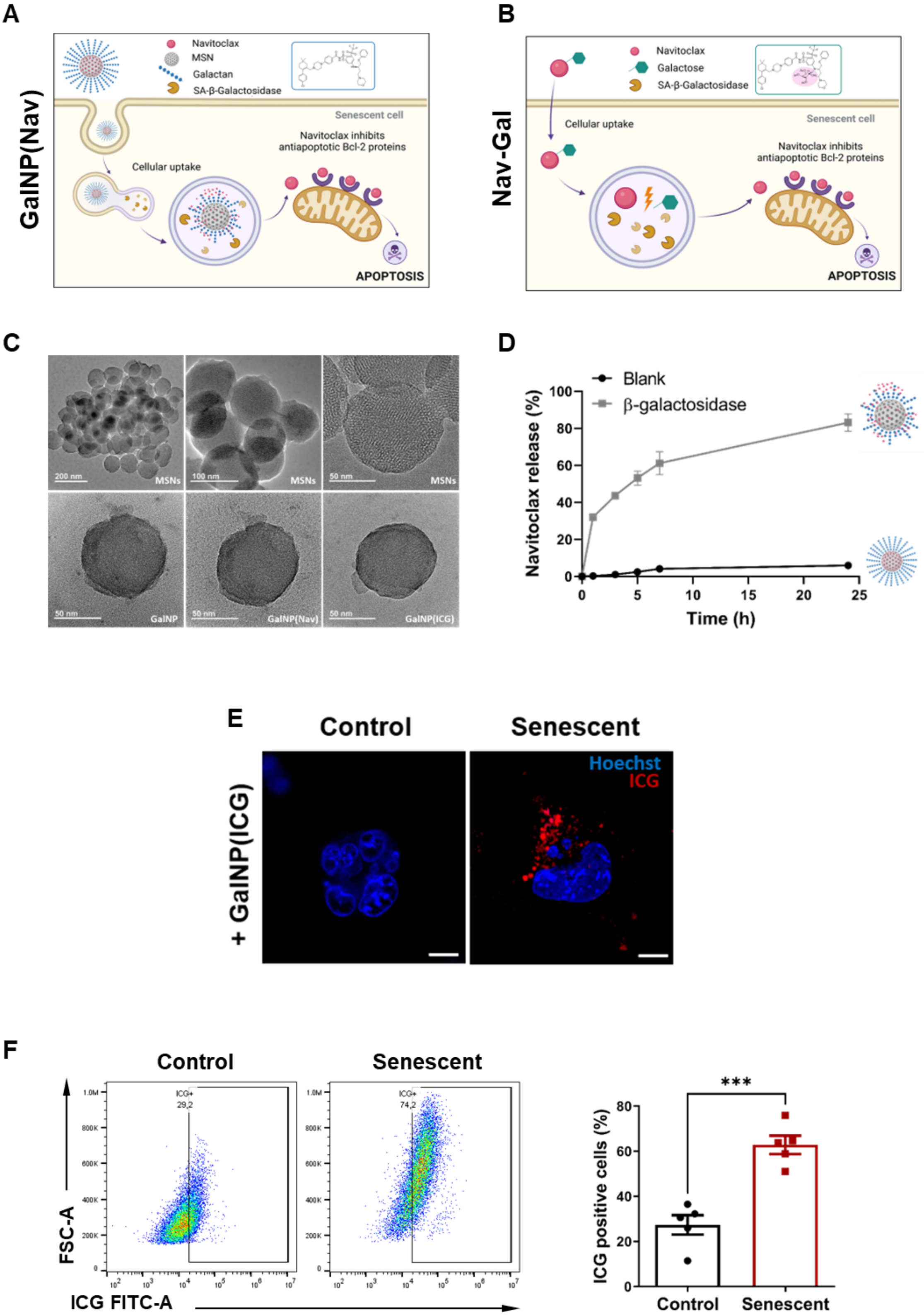

Figure 2. Characterization of synthesis and functionality of nanoparticulated systems. (A) Schematic representation of **GalNP(Nav)** based on mesoporous silica nanoparticles (MSNs) loaded with Navitoclax and coated with hexagalactosaccharide (galactan). The cellular uptake is mediated via endocytosis. **(B)** Galacto-conjugation of Navitoclax, **Nav-Gal** is passively taken

up by cells. In senescent cells, the high lysosomal β-galactosidase activity (SA-β-gal), allows the hydrolysis of either the cap or the cleavable galactose. Free Navitoclax is released into the cytoplasm and inhibits anti-apoptotic Bcl-2 proteins, which are overexpressed in senescent cells, driving specific apoptosis. **(C)** (Upper panels) TEM analysis of **calcined MSNs** at increasing magnification. (Lower panels) TEM images of **GalNP** (left), **GalNP(Nav)** (central), and **GalNP(ICG)** (right). **(D)** Release profiles of Navitoclax from **GalNP(Nav)** in the absence (blank) or the presence of β-galactosidase from *Aspergillus oryzae* in water at pH 4.5. Data represent the means ± SEM (n=3). **(E)** Confocal images of control and senescent cells incubated with **GalNP(ICG)** for 4h (1mg/ml, filtered). **GalNP(ICG)** are preferentially internalized by HL-1 senescent cells showing an increment in ICG release (red fluorescence). The nucleus is stained with Hoechst 33342 (blue). Scale bar, 10 μm. **(F)** (Left) Flow cytometry diagram of control and senescent cells incubated with **GalNP(ICG)** for 4h (1mg/ml, filtered). Increased signal for ICG indicates preferential uptake of nanoparticles in senescent cells. (Right) Percentage values of ICG positive cells obtained by flow cytometry expressed as mean ± SEM and statistical significance was assessed by the two-tailed Student's t-test: ***$p<0.001$ (n=5).

Once demonstrated the targeted delivery of the nanoparticles to senescent HL-1 cells, we evaluated the senolytic activity of **GalNP(Nav).** For this purpose, control and senescent cardiac myocytes were treated with increasing concentrations of **GalNP(Nav)** for 48h (**Figure 3A)**. We observed that HL-1 senescent cells treated with **GalNP(Nav)** showed higher sensitivity (IC50 of 0.16 μM), compared with control cells which remained viable in all the concentration range tested (up to 14 μM). The results confirmed a higher efficiency of the nanosenolytic compared with free Navitoclax (nearly 4-fold), thus resulting in a senolytic index of >86.7 (**Figure 3B, 3E**). These results show the use of **GalNP(Nav)** improved the therapeutic outcome by reducing the dose of the drug and, consequently, protecting the non-senescent cells from apoptosis.

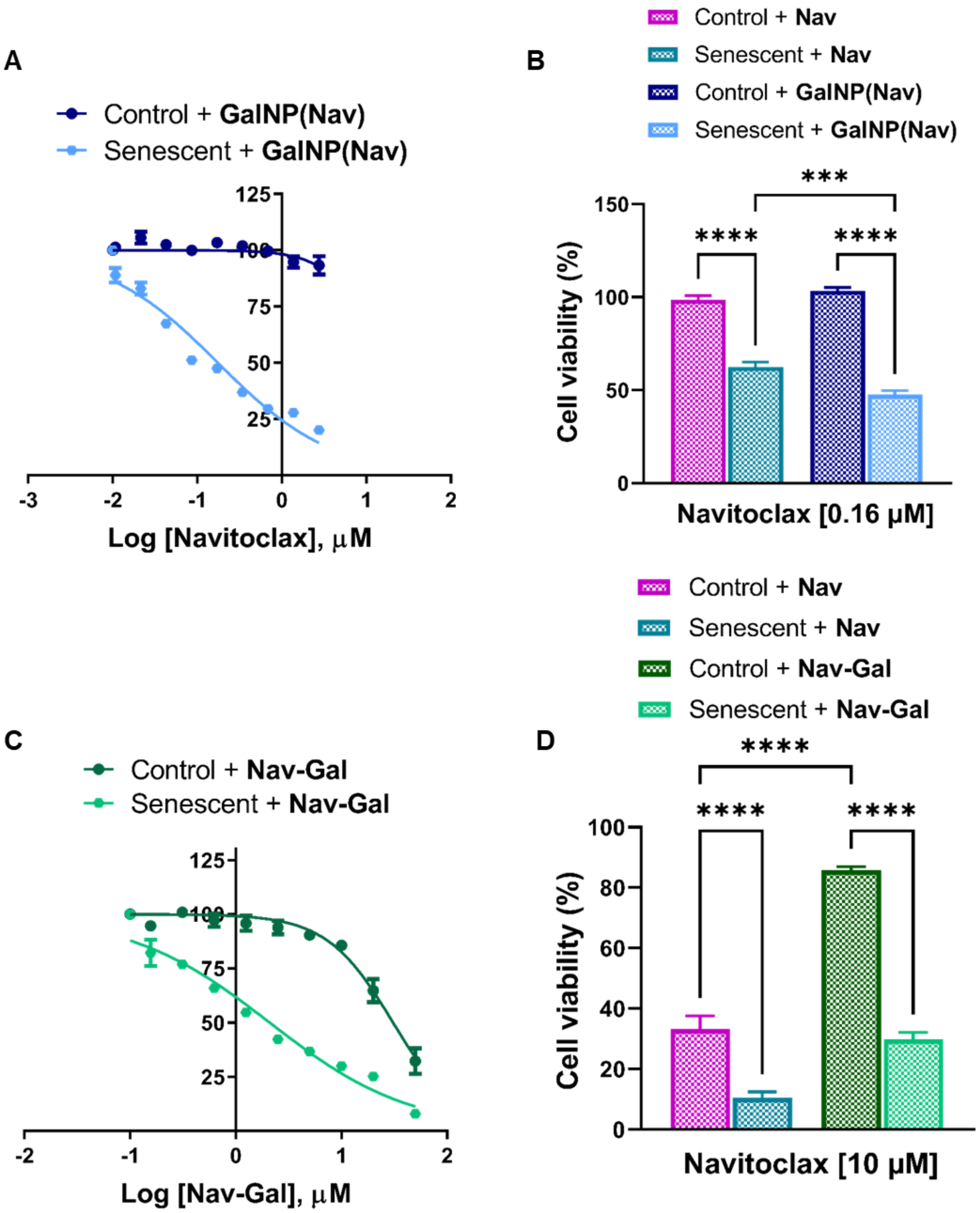

E

Senolytic	Cells	IC50 (μM)	Senolytic index
Navitoclax	**Control**	8.43	**23x**
	Senescent	0.37	
GalNP(Nav)	**Control**	>14	**>86.7x**
	Senescent	0.16	
Nav-Gal	**Control**	30.76	**14.7x**
	Senescent	2.09	

Figure 3. GalNP(Nav) and Gal-Nav improve senolytic activity over HL-1 senescent cells. **(A)** IC50 curves obtained with increasing concentrations of **GalNP(Nav)** (correlated to 0.01 to

2.7 µM of free Navitoclax) for control and DOX-treated cells measured after 48h of treatment by luminescent ATP detection. Values are expressed as mean ± SEM (n=5). **(B)** Comparison of the cytotoxic effect of free Navitoclax versus **GalNP(Nav)** over control and senescent HL-1 cells at corresponding IC50 of senescent cells treated with **GalNP(Nav)**. Data represent means ± SEM for free Navitoclax treated control and senescent cells (left), and **GalNP(Nav)** treated control and senescent cells (right). Statistical significance was determined by one-way ANOVA and Tukey post-test; $***p<0.001$; $****p<0.0001$ ($n \geq 5$). **(C)** IC50 curves obtained with increasing concentrations of **Nav-Gal** (0.15 to 50 µM) for control and DOX-treated cells measured after 48h of treatment by luminescent ATP detection. Values are expressed as mean ± SEM (n=3). **(D)** Comparison of the cytotoxic effect of free Navitoclax and **Nav-Gal** over control and senescent HL-1 cells at 10 µM. Data represent means ± SEM for free Navitoclax treated control and senescent cells (left), and **Nav-Gal** treated control and senescent (right). Statistical significance was determined by one-way ANOVA and Tukey post-test; $****p<0.0001$ ($n \geq 3$). (**E**) Table indicating IC50 (µM) values and senolytic index for different Navitoclax-based treatments in HL-1 cells. Senolytic index is obtained as $IC50^{Control}/IC50^{Senescent.}$

As an alternative to targeting Navitoclax to senescent cells, we have previously described the preparation of the prodrug **Nav-Gal** based on the conjugation of Navitoclax with an acetylated galactose (**Figure 2B**) [38]. We determine the presence of acetylated galactose in the structure of **Nav-Gal**, by nuclear magnetic resonance techniques, ^{1}H-NMR, COSY, and high-resolution mass spectrometry (HRMS) experiments (**Figure S5**). **Nav-Gal** ^{1}H-NMR spectrum (**Figure S5A**) shows the presence of 4 singlets that integrate at 3 protons for each signal. The ppm values are 2.17 (s, 3H), 2.02 (s, 3H), 2.01 (s, 3H), 2.00 (s, 3H), respectively. These values are characteristic of protons attached to alpha carbons relative to a carbonyl group. These values correspond with the 4 acetyl groups present on the galactose unit. Using two-dimensional homonuclear correlated spectroscopy (COSY), it is determined that these signals are linked to an adjacent carbon lacking protons (carbonyl carbon of the acetyl groups) so that at these values only signals are observed on the diagonal of the spectrum (**Figure S5B**). Finally, the HRMS spectrum (**Figure S5C**) obtained indicates a charge mass ratio (m/z) in the molecular ion of 1304 that correlates with the M+H of the Nav-Gal molecule when galactose has acetyl groups.

Nav-Gal prodrug was demonstrated to induce apoptosis preferentially in senescent cells, in a wide range of cell lines and models of TIS [38]. In HL-1, **Nav-Gal** showed an IC50 value of 2.1 µM for senescent HL- 1 cells and 30.8 µM for non-senescent control cells **(Figure 3C, 3E**). Albeit the senolytic index of **Nav-Gal** was slightly lower than that obtained for free Navitoclax,

Nav-Gal displays higher and remarkable protection on control cells even at high doses. For instance, at Navitoclax concentrations of 10 μM, over 65% of control HL-1 cells are dead, whereas this value was only 15% for **Nav-Gal** (**Figure 3D).** These results evidence the efficacy of the prodrug in limiting the off-target effects derived from Navitoclax and preventing non-senescent HL-1 cells from Navitoclax cytotoxic activity.

2.3. Doxorubicin induces senescence accumulation in heart tissue and cardiac dysfunction in mice

Male mice appear to be more susceptible to anthracycline cardiac toxicity than female mice. Furthermore, the mechanism behind this sexual dimorphism is unknown, and the sex-related changes in mice seem to be model-specific [39,40]. Thus, both male and female mice were included in this study. On the other hand, a single dose of 10 mg/kg DOX was previously demonstrated to induce senescence in the heart and correlated with cardiac dysfunction [7]. Nevertheless, a chronic treatment would be a more realistic approach considering the administration patterns used for patients [41]. Thus, we examined the effects of either a single dose of DOX (10 mg/kg, i.p.), henceforth referred to as DOX10, or the chronic injection of smaller doses 2 days/week at 2.5 mg/kg (accumulated dose, 20 mg/kg., i.p.), henceforth referred as DOX20, in male and female C57BL/6J mice (10-weeks). After 4 weeks of treatment, all mice were maintained free of treatment until day 44 (**Figure 4A**).

The effect of DOX on cardiac function was assessed by echocardiography (Echo). Fractional shortening (FS) indicates the change of left ventricular diameter during systolic contraction, and ejection fraction (EF) stands for the percentage of blood volume pumping capacity [7]. The echocardiographic evaluation revealed a decrease in FS (**Figure 4B and C**) and EF **(Figure S6B and C)** in DOX10-treated mice, regardless of sex, observed since day 22. In the case of the chronic regime, the decrease of FS and EF values was found preferentially in female mice, which was observable from the second week after treatment **(Figure 4C and S6B-D).** Importantly, cardiac function remained stable in control mice over the time course of this study. Representative echocardiographic images are shown in **Figures 4B, 4C, and S6D**.

To assess the gene expression of senescence and cardiotoxicity markers in this mice model, we collected the hearts of the animals at the end-point. We first evaluated the difference between sexes and found a similar trend expression in these markers in both male and female animals (**Figure SE-J**). Therefore, we consider all the data for statistical analysis (**Figure 4D-F**). We evaluated the gene expression of the classical hallmarks of cellular senescence, *p16*, *p21*, and *p53*, and the well-established SASP factors, *Ccl8*, *IL-1α*, and *TNFα* (**Figure 4**)[42,43].

We observed an increased expression of *p16*, *p21*, and *p53* in the heart tissue of DOX20-treated mice, but no significant changes were found in DOX10 compared to controls (**Figure 4D).** Moreover, immunostaining analysis showed an increased expression of p21 in heart tissue of the female DOX20 group compared to controls (**Figure 4G).** The expression profile of the SASP factors markers (*Ccl8*, *IL-1α*, and *TNFα*) indicated the upregulation in DOX20 group, which strengthens the induction of senescence in this model (**Figure 4E**). We next measured the expression of different cardiac injury markers in the heart. *Sur2a* is a marker of cardiac stress tolerance, which decreases in cardiac aging [18], and high levels of *Nppa,* reflect cardiac hypertrophy and is a marker associated with heart failure [35,44]. In line with this, we observed a significant decrease in *Sur2a* expression in DOX20-treated mice but not in DOX10 group. Significant induction of *Nppa* was observed for DOX20-treated mice (**Figure 4F**). Importantly, DOX did not cause weight loss in female mice in any administration regime. In contrast, a significant decay in weight loss was observed for male mice at both doses (**Figure S6A**). Of note, no animal died during the experiment due to DOX administration. Altogether, the results indicate that both male and female mice treated with chronic administration of DOX expressed senescence and cardiotoxicity markers in heart tissue. Therefore, we did not observe significative sex-differentiation in the DOX-induced senescence phenotype under our administration regimen.

Despite no differences observed in senescence and cardiotoxicity markers in heart tissue from both males and females, females were selected for further studies considering the significant differences in cardiac function. Besides, the evaluation of cardiotoxicity in females could be a key point as anthracyclines are the backbone of chemotherapy-based regimens for breast and ovarian neoplasms [45].

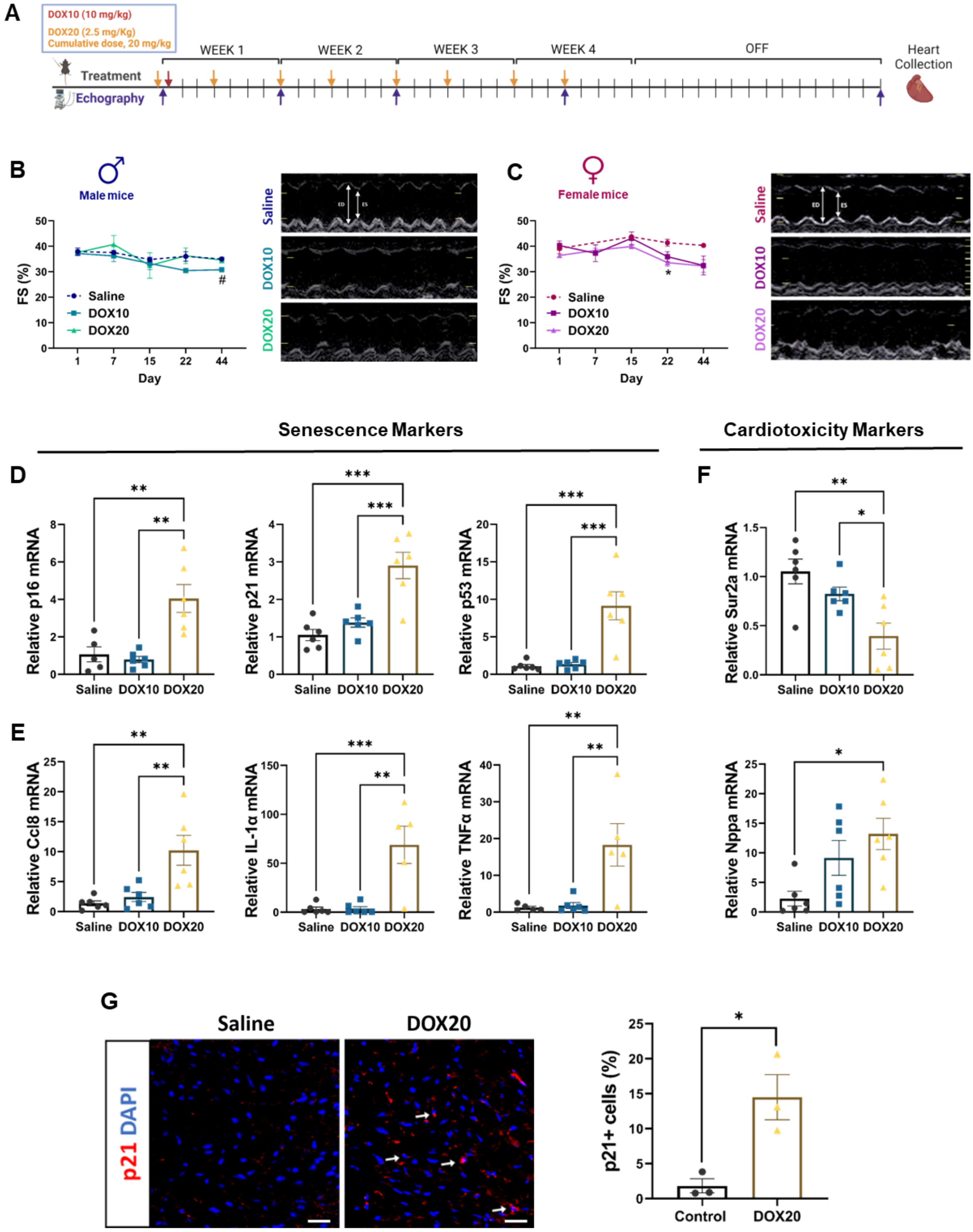

Figure 4. Doxorubicin induces senescence and cardiotoxicity markers expression in heart tissue and cardiac dysfunction in mice. (A) Experimental design: wild-type male and female C57BL/6J mice (10 weeks old) were treated with saline or doxorubicin (i.p) in a unique administration (10 mg/kg body weight, DOX10) or in a chronic regime (cumulative dose, 20 mg/kg body weight, DOX20), 2 injections per week for 4 weeks (n=3). Echocardiography analyses were performed weekly to follow the cardiac dysfunction of mice. Hearts were collected at the end-point of the experiment (day 44). The graphs representing male results are

shown in blue colors, and female results are shown in violet colors. **(B)** Fractional shortening (FS) values obtained for male animals during the curse of the experiment. A decrease in FS was observed for animals in the DOX10 group versus saline-treated mice at day 44. Data represent independent measurements for each animal (n=3). Statistical significance was determined by one-way ANOVA and Tukey post-test; #p<0.05 represents significance DOX10 vs Saline-group. **(C)** Fractional shortening (FS) values obtained for female animals during the curse of the experiment. A decrease in FS value was observed for animals in both experimental groups, DOX10 and DOX20 versus saline-treated mice. Data represent independent measurements for each animal (n=3). Statistical significance was determined by one-way ANOVA and Tukey post-test; *p<0.05 represents significance DOX20 vs Saline-group. Representative echocardiographic analysis on male and female mice, respectively, in each experimental condition at day 44 (ED = end-diastole, ES = end-systole). After injection with DOX, a decrease in LV contraction is observed. (**D-F**) mRNA expression levels of the senescence makers (**D**), *p16*, *p21*, and *p53*; SASP markers (**E**), *Ccl8, IL-1α*, and *TNFα;* and cardiotoxicity markers (**F**) *Sur2a* and *Nppa*, in heart tissue of mice. *Actb* and *Gapdh* were used for input normalization. Values are relative to control mice and are expressed as mean ± SEM. Statistical significance was determined by one-way ANOVA and Tukey post-test; *p <0.05; **p<0.01; ***p<0.001 (n≥5, heart per group). **(G)** Representative confocal images of heart tissue sections from female animals treated with saline or chronic administration of DOX (20 mg/kg). p21 expression (white arrows) is overexpressed in DOX-treated mice (red signal). DAPI (blue signal) counterstained for nucleus. Scale bar, 20 μm. Quantification of the total number of p21-positive cells. Fields were selected for covering most of the total heart area. Data represent means ± SEM per animal and statistical significance was assessed by the two-tailed Student's t-test: *p<0.05 (n=3, heart per group).

2.4. Navitoclax in different formulations restores cardiac function in a doxorubicin-induced cardiotoxicity mouse model

Navitoclax in different formulations was tested in the DOX-induced cardiotoxicity model described in the previous section. Female mice were treated with either saline (control) or DOX on days 1 and 4 every week, for 4 weeks (accumulative dose, 20 mg/kg). Senolytic treatment with either free Navitoclax (50 mg/kg/day, o.g) [26], **GalNP(Nav)** (0.025 mg/day, i.p) or **Nav-Gal** (67 mg/kg/day, i.p) were administered for 2 consecutive days following DOX administration (**Figure 5A**). According to the results above, we found a decline in cardiac function expressed by a decrease in FS and EF percentages for DOX treated groups during the experimental which were found significant at day 15 (**Figure S7A-D**). At the end-point, while FS and EF progressively declined in DOX-treated mice, a protective effect in cardiac function was observed from all three Navitoclax formulations (**Figure 5C and Figure S7E**). **Figure 5B** shows representative M-mode echocardiography images from the mice groups under study.

According to our previous results, the expression of the senescence markers *p16, p21*, and *p53* were upregulated in cardiac tissue after DOX treatment compared to control mice. Interestingly, the expression of these senescence markers was alleviated upon senolytic treatment, regardless of the therapeutic strategy used (free Navitoclax, **GalNP(Nav),** or **Nav-Gal)** (**Figure 5D**). These results were further corroborated in heart tissue by p21 and p53 immunofluorescence (**Figure 5E)**, where it was found that the induction of both markers in heart tissue after DOX treatment was reverted upon senolytic administration. Besides, a decrease in mRNA expression levels of the cardiotoxicity marker *Sur2a* upon DOX treatment was prevented upon senolytic treatment **(Figure 5G**). In addition, no evidence of losing weight, renal or hepatic damage was observed in any of the groups treated with free Navitoclax, **GalNP(Nav),** or **Nav-Gal**, as evaluated by serum markers (**Figure S7F-H**). These data support the role of senescence in cardiac dysfunction following DOX treatment and demonstrate that senolytic treatment with different formulations of Navitoclax (free, encapsulated, or as a pro-drug) restores cardiac function in mice.

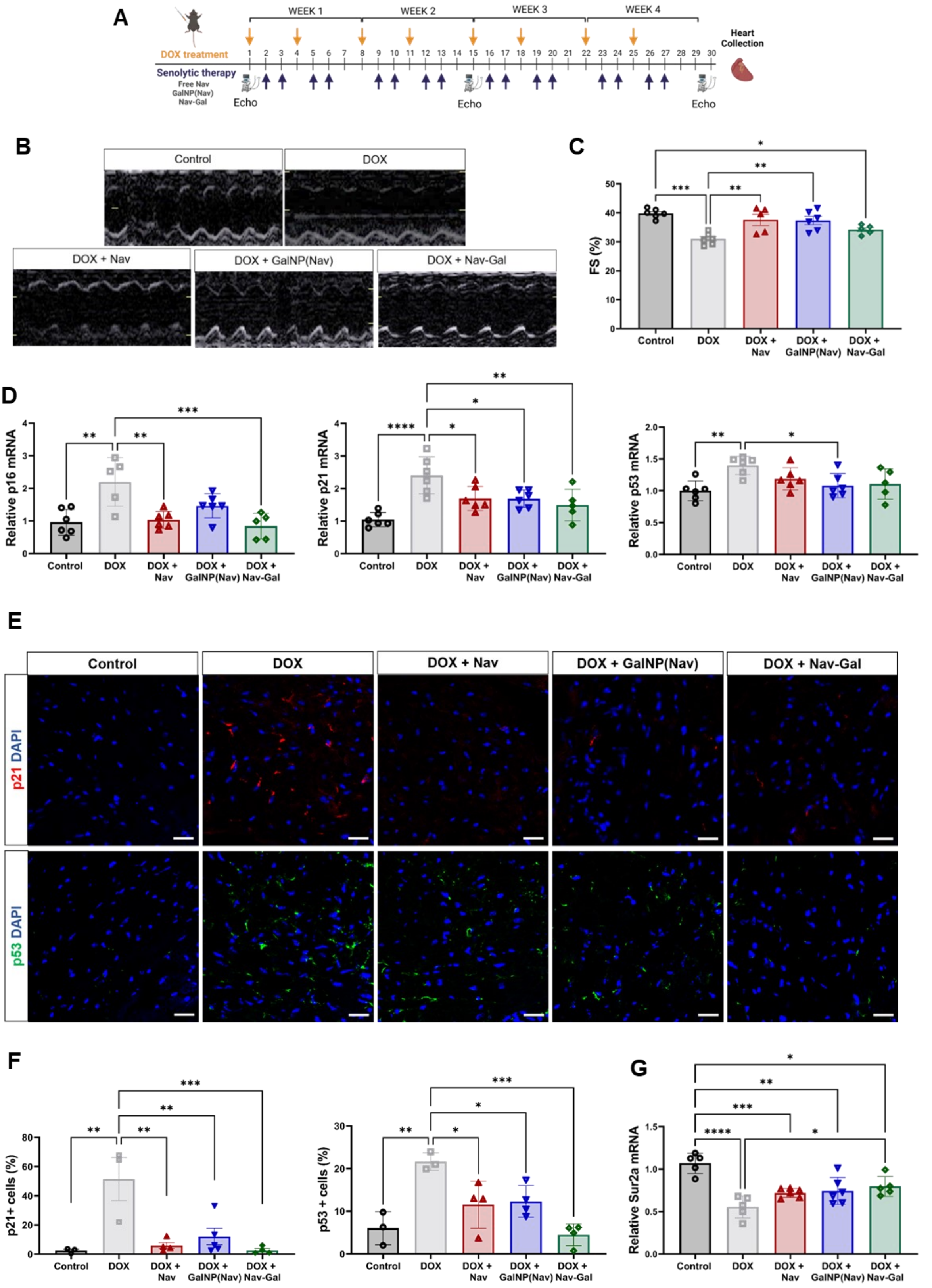

Figure 5. Navitoclax-based therapies in a doxorubicin-induced cardiotoxicity model. (A) Experimental design: wild-type female C57BL/6J mice (10 weeks old) were treated with doxorubicin (i.p) in a chronic regime (cumulative dose, 20 mg/kg body weight), 2 injections per week for 4 weeks. Senolytic treatment with either free Navitoclax (50 mg/kg/day, o.g.),

GalNP(Nav) (0.025 mg/day, i.p) or **Nav-Gal** (67 mg/kg/day, i.p) were administered for 2 consecutive days following DOX administration. Echocardiography analyses were performed every 15 days to follow the cardiac dysfunction of mice. Hearts were collected at the end-point of the experiment (day 30). C57BL/6J mice in each experimental condition (n=6) as described: Control (black), DOX (grey), DOX + Nav (red), DOX + GalNP(Nav) (blue) or DOX + Nav-Gal (green). **(B)** Representative echocardiographic analysis of mice in each experimental condition displaying changes in left ventricle (LV) systolic function at day 30. After injection with DOX, a decrease in LV contraction is observed which is attenuated upon senolytic treatment. **(C)** Fractional shortening (FS) values were obtained for animals at the experimental end-point (day 30). A decrease in FS values was observed for animals in the DOX group and FS increase upon administration of senolytic treatment. Data represent the means of 3 different independent measures for each animal ± SEM ($n \geq 5$). Statistical significance was determined by one-way ANOVA and Tukey post-test; *$p<0.05$; **$p<0.01$; ***$p<0.001$. (**D**) mRNA expression of the senescence markers *p16*, *p21*, and *p53* in the hearts of mice in each experimental condition. *Actb* and *Gapdh* were used for input normalization. Values are expressed as mean ± SEM ($n \geq 5$). Statistical significance was determined by one-way ANOVA and Tukey post-test; *$p<0.05$; **$p<0.01$; ***$p<0.001$; ****$p<0.0001$. (**E**) Representative images obtained for detection of p21 (red signal) and p53 (green signal) on heart tissue slices. DAPI stains the nucleus (blue). DOX-treatment upregulates the expression of both markers in heart tissue indicating accumulation of senescent cells. Upon administration of senolytic treatment, this upregulation is reverted. Scale bar, 20 µm. (**F)** The graphs indicate the percentage of p21-positive cells and p53-positive cells in the hearts of animals in different studied groups. Fields for quantification were selected for covering most of the total heart area. Data represent means ± SEM per animal and statistical significance was determined by one-way ANOVA and Tukey post-test; *$p<0.05$; **$p<0.01$; ***$p<0.001$; ****$p<0.0001$ ($n \geq 3$ hearts per group). (**G**) mRNA expression levels of the cardiotoxicity marker *Sur2a* maker in the hearts of mice in each experimental condition. *Actb* and *Gapdh* were used for input normalization. Values are expressed as mean ± SEM ($n \geq 5$). Statistical significance was determined by one-way ANOVA and Tukey post-test; *$p<0.05$; **$p<0.01$; ***$p<0.001$; ****$p<0.0001$

3. Discussion

The clinical use of doxorubicin (DOX) is hindered due to the development of irreversible cardiotoxicity and is a growing epidemiologic problem [10]. Although the mechanism of DOX-induced cardiotoxicity stays not fully understood, the main hypothesis suggests that oxidative stress is the primary cause of DOX-induced cardiomyopathy [9,46]. However, protective antioxidant approaches, such as dexrazoxane, only confer some level of cardioprotection in clinically relevant trials suggesting that efficacious therapy may require more specific targeting strategies to provide long-term cardioprotection [47,48]. Previous reports have established that DOX-induced cell senescence in the heart correlates with worse cardiac outcomes in patients [13,14], and the genetic clearance of p16INK4A-expressing senescent cells improved cardiac function in DOX-treated mice [7]. Other studies found that Navitoclax favors the elimination of senescent cells accumulated in the heart in mice models of aging, myocardial infarction, and ischemia-reperfusion, and can reverse pathologic-associated phenotypes [6,25,26]. Considering these findings, it exists a clear potential for using senolytics as a protective strategy for DOX-associated cardiotoxicity. However, such an appealing concept has never been demonstrated.

For the *in vitro* study of senescent cardiomyocytes, the primary isolated cardiomyocytes seem to exhibit the best similarity to *in vivo* features [49], nevertheless, their use in culture is limited. Thus, immortalized cell lines as HL-1 cells offer alternative approaches for drug evaluation although animal models continue to be an essential tool for studying cardiac senescence. In this study, we proved that treatment with DOX efficiently induces senescence in the HL-1 myocyte cell line and the heart of C57BL6/J mice treated with a cumulative dose of DOX (20 mg/kg administered in 8 doses of 2.5 mg/kg for 4 weeks, i.p.). DOX induces the expression of classical hallmarks of cellular senescence and well-established senescence-associated secretory phenotype (SASP) factors, in both the *in vitro* and the *in vivo* models [7,12,42]. No sex differences were observed in the gene expression of senescence and cardiotoxicity markers in heart tissue, but we found significant differences in cardiac function when female mice were treated with chronic DOX administration. Therefore, due that DOX being usually administered for the treatment of breast and ovarian human cancers, we selected females for further studies.

We next evaluated a senolytic strategy for the elimination of senescent cells based on the use of the senolytic Navitoclax in different formulations. Senolytic therapies are not exempt from off-target toxicities in normal cells, thus, specifically targeting senescent cells remains a considerable challenge. Therefore, we studied not only free Navitoclax administration but also two targeted therapies to overcome undesired side-effects and toxicities of free Navitoclax [27]. Both targeted therapies are based on the high level of lysosomal β-galactosidase activity in senescent cells [30]. We previously demonstrated that encapsulated Navitoclax in mesoporous silica nanoparticles (MSNs) capped with galactan effectively releases the cargo within senescent cells [36]. In fact, the treatment of senescent HL-1 cells with **GalNP(Nav)** increases the senolytic index of free Navitoclax, in agreement with previous reports in chemotherapy-induced senescence tumor models [35–37]. Despite these promising results and the emergent interest in nanomedicine applications, the clinical translation of nanotechnologies is still challenging due to an incomplete understanding of nano-bio interactions and scalable manufacturing [50]. As an alternative to nanotechnology, we also functionalized Navitoclax with a cleavable acetylated galactose, obtaining the prodrug **Nav-Gal**. The prodrug had been previously validated in tumor models of chemotherapy-induced senescence and demonstrated an improved selective senolytic activity [38]. The senolytic index of **Nav-Gal** for HL-1 cells was slightly lower than that obtained for free Navitoclax. However, the advantage of **Nav-Gal** relies on the remarkable low toxicity on non-senescent HL-1 cells.

Accordingly, mice administered with concomitant treatment of DOX and senolytics (free Navitoclax, galacto-functionalized Navitoclax-loaded MSNs (**GalNP(Nav)**), or as prodrug (**Nav-Gal**)), show a reduced accumulation of senescence in the heart, demonstrated by expression of the senescence markers *p16, p21*, and *p53*, and an attenuated cardiac injury shown by the expression of *Sur2a*. Of note, this senescent cell clearance correlates with a preserved cardiac function. Mice treated with DOX exhibit a decrease in cardiac functionality, evidenced by the reduction in fractional shortening and ejection fraction, which were attenuated upon senolytic treatment, making the results obtained from this study particularly relevant [51]. Importantly, it is remarkable that Navitoclax dose was 40 times lower when encapsulated in **GalNP(Nav)**, displaying a similar therapeutic effect to free Navitoclax. Of note, previous studies on the use of **GalNP(Nav)** and **Nav-Gal** on senescent cancer mouse models [35,38], demonstrated these strategies protected from a significant reduction in platelet counts associated to free Navitoclax in treated mice and human and murine blood samples. Notably, wild-type C57BL/6J mice treated for 10 consecutive days with **Nav-Gal** resulted in less thrombocytopenia compared to free Navitoclax treatment [38].

Observed differences between Navitoclax, **GalNP(Nav),** and **Nav-Gal** *in vitro* are likely due to the built-in mechanism for the targeted therapy, which requires previous processing and activation by lysosomal β-galactosidase activity, meaning that Navitoclax and its targeted-based therapies might have different pharmacokinetics and pharmacodynamics. It is worth noting that the *in vitro* assays do not always fully recapitulate what happens *in vivo* due to the complexity of living organisms. Thus, regarding the *in vivo* assays, the therapeutic window is comparable for the 3 senolytic alternatives. As the administration of **Nav-Gal** was molar equivalent to Navitoclax, we observed similar therapeutical behavior. Of note, the advantage of using **Nav-Gal** resides in the prevention of the off-target effects associated with the free drug administration. In the case of **GalNP(Nav)**, the use of a nanocarrier increases the bioavailability of the drug in the target organ, reducing doses and, therefore, side-effects. Thus, we observed similar results when compared to its counterparts even when 40x lower dose was administered. In conclusion, the main advantage of both targeted therapies resides in reducing off-target effects and preventing associated side-effects such as thrombocytopenia, which is highly desirable for clinical applications. Nonetheless, because clinical studies might be simpler to conduct, it will be likely for the prodrug formulation to reach clinical applications first. Nevertheless, note that silica nanoparticles have already reached clinical trials evaluation and thus the use of MSNs in clinics could be expected in the near future [52,53].

Previous works have shown that senotherapies have the potential to reverse age-related dysfunction in cardiac tissues through the promotion of regenerative capacity [6,23]. We suggest that the therapeutic effect of Navitoclax in our experimental model (regardless of the formulation used) could be explained as follows: i) DOX produces DNA damage and oxidative stress which induces accumulation of damaged cells in the heart and leads to senescence; ii) accumulated senescent cells release SASPs factors promoting a proinflammatory microenvironment and accelerated aging, and lead to myocardial dysfunction; iii) senolysis acts as an adjuvant therapy favoring senescent cells elimination and preventing from the associated cardiotoxicity; iv) the eradication of senescent cells might also mitigate the senescent secretome (SASP), avoiding bystander effect; v) selective elimination of senescent cells with senolytic alleviate cardiac deterioration by doxorubicin and promote the regenerative capacity of the heart.

Altogether, we report here the first demonstration that systemic administration of Navitoclax in different formulations is effective in clearing senescent cells in the heart and correlates with the prevention of cardiac dysfunction in a mouse model of doxorubicin-induced cardiotoxicity. These results evidence the potential of using these new senolytic therapies to alleviate cardiac dysfunction, thus limiting the cardiotoxicity induced in DOX-treated patients. Selective elimination of senescent cells with senolytics could become a promising next-generation therapy to address an unmet medical need in cardiac pathologies. The study also supports that the combination of senolytics with anticancer agents used in clinics might reduce accelerated aging processes and adverse side-effects induced by chemotherapy in patients in different tissues and organs.

4. Experimental section

1. Synthesis of nanoparticles

A typical synthesis of MSNs was carried out using N-cetyltrimethylammonium bromide (CTAB, Sigma, #H6269) and tetraethylorthosilicate (TEOS, Sigma, #131903) to prepare the as- synthesized MSNs as described [34]. Briefly, a CTAB solution (1g, 2.74 mmol) was prepared in deionized H_20 and NaOH solution (3.5 mL, 2 M. Sigma, #1310732) was then added. The surfactant solution was stirred at 80°C and TEOS (5 mL, 2.57 x 10^{-2} mol) was added dropwise. The mixture continued stirring for 2h to give a white precipitate. The solid was isolated by centrifugation (10,000 rpm, 20 min) and washed with deionized H_20 until neutral pH. The material was dried at 80°C overnight, obtaining de porous scaffold “as made” MSNs. Then, “as made” MSNs were calcined at 550°C in an oxidant atmosphere to remove the CTAB template, obtaining de porous scaffold “calcinated” MSNs.

Synthesis of gated MSNs coated with a hexagalactosaccharide (galactan) (Megazyme, #P-GALPOT), composed of six repeating galactose monosaccharides linked through β-1,4 glycosidic bonds, and loaded with Navitoclax (Active BioChem, #A1001) or indocyanine green (ICG, Sigma, #I2633) was performed as described previously [37]. For **GalNP(ICG),** 9.3 mg of ICG were dissolved in 67.5 mL of water at a pH of 7.5 and 200 mg of calcined MSNs were added. The mixture was stirred for 24 h at room temperature, and the nanoparticles were filtered and dried under vacuum (**NP(ICG)**). Then, an excess of (3-aminopropyl)triethoxysilane (APTES) (6 mmoles/g solid, 0.28 mL) dissolved in 6 mL of acetonitrile was prepared and the NP(ICG) obtained were added to the solution. After stirring for 5.5 h at room temperature the functionalization of the external surface was completed and the solid (**NP(ICG)-NH_2**) was isolated by filtrations under vacuum. For the synthesis of **GalNP(Nav)**, the nanoparticles were loaded with Navitoclax by the addition of 156 mg of this drug to a suspension of 200 mg of calcined MSNs in 6 mL of anhydrous dichloromethane under argon atmosphere. After 24 h of stirring, 0.28 mL of APTES were added to the suspension and the stirring was kept for further 5.5 h under argon atmosphere. Then, the solid was filtered and isolated under vacuum (**NP(Nav)-NH_2**). On the other hand, NP-NH_2 was synthesized by adding 0.28 mL of APTES to a suspension of 200 mg of empty calcined MSNs in 6 mL of anhydrous acetonitrile. After 5.5

h, the functionalized solid was isolated by filtration under vacuum. For coating MSNs with galactan, the obtained solids functionalized with amino moieties were added to a solution of 383 mg of galactan in 25 mL of water, and stirring was continued at room temperature for 21 h. After stirring for 21h at RT, the final product, referred to as **GalNP(ICG), GalNP(Nav),** and **GalNP(0),** was filtered, washed with plenty of water and ethanol, and dried under vacuum. All the final nanoparticles were stored in a desiccator at room temperature.

2. *Characterization of prepared nanoparticles*

Powder X-ray diffraction (PXRD), TEM, N_2 adsorption-desorption, thermogravimetric analysis, dynamic light scattering (DLS), and HPLC measurements were employed to characterize the prepared materials. PXRD was performed on a Seifert 3000TT diffractometer using CuKα radiation at low angles ($1.3 < 2\theta < 8.3$, with steps of 0.04 degrees and 3 seconds for step) and high angles ($35 < 2\theta < 80$, with steps of 0.04 degrees and 1 second for step). For TEM, images were acquired in a Philips CM-10. Samples were deposited on copper grids covered with carbon film provided by Electron Microscopy Sciences to obtain high-resolution images. Micrographs were captured with 200 KV in a JEOL JEM-2100F microscope equipped with an X-ray detector. N_2 adsorption-desorption isotherms were recorded on a Micromeritics TriStar II Plus automated analyzer. Samples were previously degassed at 40°C in vacuum overnight and measurements were performed at 77K. The specific surface areas were calculated from the adsorption data in the low pressures range using the BET model. Thermogravimetric analysis (TGA) was carried out on a TGA/SDTA 851e Mettler Toledo equipment, using an oxidant atmosphere (air, 80 mL/min) with a heating program consisting of a heating rate of 10°C/min from 393K to 1273K and an isothermal heating step at this temperature for 30 min. Pore size was determined by following the BJH method. DLS measurements were carried out in a Malvern Zetasizer Nano ZS. UV-visible spectroscopy was carried out with a Lambda 35 UV/Vis spectrometer (Perkin-Elmer Instruments) and fluorescence spectroscopy was performed with a JASCO spectrofluorometer FP-8300.

3. *Cargo release studies*

To assess the proper working of the capping ensemble 4 mg of **GalNP(Nav)** were suspended in 10 mL of water at pH 4.5, stirred, and separated into two suspensions of 5 mL. Then, 7 mg of β-galactosidase from *Aspergillus oryzae* were added to one of the aliquots. After a certain time, 200 μL of each suspension was taken and 300 μL of ethyl acetate was added to each one, stirred for 1 min and the organic phase was taken, cargo released in the organic phase was measured by UV-visible spectroscopy (Navitoclax absorption band in ethyl acetate at 275 nm). Cargo release studies from **GalNP(ICG)** were obtained following a similar procedure. An aliquot of 300 μL of the suspension was taken at a determined time and 2 μL of NaOH (0.15 M) was added to the aliquot. The suspension was vigorously stirred for 3 min and centrifuged for removing the solid. Then, release was measured by fluorometric spectroscopy (λ_{exc} (ICG) = 775 nm, λ_{em} (ICG) = 805 nm). To acquire a "blank" control, the same approach was carried out without the addition of enzyme onto the other suspension.

4. Synthesis of Nav-Gal prodrug

Nav-Gal was synthesized following the literature procedure [38]. Briefly, 40 mg (0.04 mmol) of Navitoclax (Eurodiagnostico), 25 mg (0.06 mmol) of 2,3,4,6-tetra-O-acetyl-alfa-D-galactopyranosyl-bromide (Sigma), and 23 mg (0.17 mmol) of K_2CO_3 (Sigma) were mixed, and the solids were purged with argon. Anhydrous acetonitrile 10 mL (Sigma) was added, and the mixture was stirred at 70°C for 3h under an argon atmosphere. The solvent was removed under vacuum pressure. The crude product was purified by flash chromatography on silica gel (Sigma), from hexane-ethylacetate (3:7 v/v; Scharlab) to hexane-ethylacetate (7:3 v/v) used as eluent. Purified Nav-Gal was obtained as a yellow powder in a 35% yield. For *in* vivo mice experiment, some batches were mixed before to purified by flash column. Characterization of the prodrug was evaluated by ^{1}H-NMR, two-dimensional homonuclear correlated spectroscopy (COSY), and the HRMS spectrum as indicated in the text.

5. Cell culture and senescence induction

HL-1 Cardiac Muscle Cell Line was obtained from Sigma (SCC065) and was grown, as protocol detailed, in fibronectin (Sigma, F1141) coated flasks containing Claycomb medium (Sigma, 51800C) and supplemented with 10% fetal bovine serum (FBS) (Sigma, F7524), 2 mM L-glutamine (Sigma, G7513) and 0.1 mM norepinephrine (Sigma, A0937). Cells were incubated at 37°C in an atmosphere of 5% CO_2 and 95% air. For senescence induction, cells were supplemented with a medium containing Doxorubicin (Carbosynth, AD15377) at 100 nM for 3 days. Cells were routinely tested for mycoplasma contamination.

6. β-galactosidase activity assay

β-galactosidase staining was performed in cells using the Senescence β-galactosidase Staining Kit (Cell Signaling, #9860) following the manufacturer's instructions. Briefly, cells were fixed at room temperature for 10 min with a solution containing 2% formaldehyde and 0.2% glutaraldehyde in PBS, stained with the X-gal Staining Solution (pH 6.0), and incubated overnight at 37°C without CO_2. Cells were then detected for blue staining under a bright-field microscope.

7. $C_{12}FDG$ determination by flow cytometry

To quantify β-galactosidase activity by flow cytometry, the fluorogenic substrate $C_{12}FDG$ (Santa Cruz Biotechnology, Inc., # sc-284621A) was used [54]. Control and senescent HL-1 cells were seeded in a 6-well culture plate. The following day, cells were pretreated with 0.1 mM bafilomycin A1 for 1h to induce lysosomal alkalinization in a fresh culture medium. Cells were washed with PBS and treated with 5-dodecanoylaminofluorescein di-b-D-galactopyranoside ($C_{12}FDG$) (S.Cruz Biotechnology, #sc-284621A), 33 μM for 3h at 37 °C under 5% CO_2. Next, cells were washed with PBS and harvested by adding 0.5% Trypsin-EDTA (GIBCO). Cells were collected, centrifuged, and resuspended in PBS. Flow cytometry assay was carried out on a CytoFlex S instrument (Beckman Coulter) followed by data analysis using CytoExpert software.

8. Cell cycle assay

For the cell cycle evaluation assays, control and DOX-treated HL-1 cells (3 days at 100 nM) were fixed and permeabilized with ethanol for 1h at -20 °C. Then, cells were centrifuged and 0.5 mL of PI/RNAse buffer solution from Immunostep were added to each control or DOX-treated cells (1 x 10^6 cells) and incubated overnight at 4°C before analysis. Samples were acquired by flow cytometry using the CytoFLEX S Beckman Coulter and analyzed by FlowJo software.

9. Cell proliferation

Time-lapse images were acquired for control and DOX-treated HL-1 cells (3 days at 100 nM) seeded in p96-multiwell plates at a density of 15.000 using Cytation 5 Cell Imaging Multi-Mode Reader while maintained in BioSpa8 (BioTek, USA). Images were taken every 3 h up to 48 hr and were analyzed for confluence increment using BioTek Gen5 Data Analysis Software.

10. Ki67 immunofluorescence

Control and senescent cells were seeded on coverslips and fixed in 4% PFA for 10 min, permeabilized with 0.3% Triton X-100 and blocked with 5% BSA for 1h. Cells were incubated with primary antibody solution (1% BSA, 0.3% Triton X-100) containing anti-Ki67 (D3B5) (1:500, Cell Signaling, #9129) overnight at 4ºC. The next day, samples were incubated with Alexa anti-rabbit IgG Fluor Goat 633 (1:100, Fisher, #A21071) for 2h at room temperature in darkness. For image visualization coverslips were mounted on glass slides with mounting Hoechst staining solution and visualized in Leica TCS SP8 HyVolution 2 confocal microscope.

11. Clonogenic assay

For clonogenic assay, control and senescent cells were seeded at increasing cell densities in a 24-well plate and incubated at 37°C in an atmosphere of 5% CO_2 and 95% air for 1 week. Then, cells were washed with PBS and fixed with 4% PFA for 10 min and stained with 0.05% crystal violet for 45 min, and the excess was washed with deionized water. Images were taken under a bright-field microscope.

12. Western blot

Both control and DOX-treated cells were scraped-harvested in lysis buffer (25mM Tris-HCl pH 7.4, 1mM EDTA, 1mM EGTA, SDS 1%, and protease and phosphatase inhibitors), passed through a 25G needle, and boiled for 10 min to prepare whole-cell extracts. Protein quantification was performed using a BCA protein assay. An identical amount of whole-cell extracts (70 µg) was resolved in 8-12% SDS-PAGE gels, transferred to nitrocellulose membranes (GE Healthcare, #10600002), and blocked with 5% skimmed milk solution for 1 h. Membranes were incubated at 4°C overnight with primary antibodies (data below). The expression of GAPDH was detected in cell lysates as a reference protein for normalization. Membranes were washed with 0.1% Tween/PBS and incubated with the appropriate secondary antibody conjugated with horseradish peroxidase for 2h at room temperature. Immunoblot signals were detected using GE Healthcare's ECL chemiluminescence detection reagents using the Amersham Imager 600 equipment. *Antibodies:* anti-phospho-Rb (Ser780) (1:1000, Cell Signaling, #9307); anti-β-Galactosidase (E2U2I) (1:1000, Cell Signaling #27198); anti-p21 (1:1000, Santa Cruz, #sc-6246); anti-p53 [PAb 240] (1:1000, Abcam, #ab26); anti-Bcl-2 (50Ee) (1:1000, Cell Signaling, #2870); anti-Bcl-xL (1:1000, Cell Signaling, #2764); anti-Bcl-w (31H4) (1:1000, Cell Signaling, #2724); anti-Bim (1:1000, Cell Signaling, #2819); anti-Bok (Abcam, ab186745), anti-GAPDH (14C10), (1:1000, Cell Signaling, #2118). The secondary antibodies used were anti-Rabbit IgG peroxidase antibody (Sigma, #A6154) and peroxidase conjugate-goat anti-Mouse IgG antibody (Sigma, #A4416).

13. Cytotoxicity cell studies

For DOX dose-response, HL-1 cells were seeded in flat-bottom clear white p96-multiwell plates (PerkinElmer #6005181) at a density of 15,000. The next day, cells were treated with different concentrations of DOX (0.05 – 1 µM) for 72 h. The cytotoxic effect of free Navitoclax, **GalNP(Nav)**, **Nav-Gal,** and **GalNP(0**) was evaluated for control and senescent HL-1 cells seeded in flat-bottom clear white p96-multiwell plates at a density of 15,000 and 25,000 cells/well, respectively. The following day cells were treated with serial dilutions of Navitoclax, **GalNP(Nav)**, **Nav-Gal,** or **GalNP(0**) (0.015-50 µM for Navitoclax and **Nav-Gal**; 0.015-2 mg/mL, which corresponds to 2.7 µM maximal concentration, for **GalNP(Nav)** and **GalNP(0)** previous filtration in 0.45 µM and were incubated for 48h. All viability assay was assessed by measuring luminescence with CellTiter-Glo Luminescent Cell Viability Assay (Promega, #G7571) following the manufacturer's instructions in a Wallac Victor2TM plate reader spectrophotometer (PerkinElmer). The number of viable cells was normalized to the internal control of untreated cells (vehicle only), either control or DOX-treated cells for each plate. Non-linear fit log(inhibitor) versus response with a variable slope (four parameters) model was used for IC50 estimation in GraphPad 9.0 software.

14. Targeted cellular uptake study

The targeting features of the prepared materials were evaluated in control and senescent HL-1 cells by confocal microscopy and flow cytometry. For image acquisition by confocal, cells were seeded on a coverslip in a 6-well plate at a concentration of 200,000 cells/well. The next day, a suspension of 1mg/ml **GalNP(IGC)** was resolved in culture medium, previously sonicated, stirred for 45 min, and filtered in a 0.45 µm. The NPs dispersion was added to the cells and incubated for 4h. Medium with NPs was removed, and cells were washed with PBS to eliminate non-internalized NPs. The coverslips were mounted, and Hoechst 33342 was added for nuclei staining. Cells were visualized in Leica TCS SP8 HyVolution 2 confocal microscope. A similar procedure was assessed for flow cytometry quantification. After treatment, cells were collected by adding 0.5% Trypsin-EDTA (GIBCO), centrifuged, and resuspended in PBS. Flow cytometry assay was carried out on a CytoFlex S instrument (Beckman Coulter) followed by data analysis using CytoExpert software. Senescence autofluorescence was also considered (by subtracting it).

15. Mouse experiments

Animals used in this study were purchased from Charles River Laboratories and maintained in ventilated racks under pathogen-free conditions at Principe Felipe Research Centre (Valencia, Spain), with food and water ad libitum and alternate dark and light cycles. All animals were treated humanely, and experiments were approved by the Ethical Committee for Research and Animal Welfare Generalitat Valenciana, Conselleria dÀgricultura, Medi ambient, Canvi climàtic i Desenvolupament Rural (2020/VSC/PEA/0217). To establish the mouse model of doxorubicin-induced cardiotoxicity associated with cardiac senescence wild-type male and female C57BL/6J mice (strain code: 632) (10 weeks old) were used. DOX was administered intraperitoneal (i.p.) once with 10 mg/kg of doxorubicin hydrochloride (Carbosynth, AD15377) in saline (groups DOX10) or eight equal intraperitoneal injections (2.5 mg/kg) for 4 weeks with a total cumulative dosage of 20 mg/kg, (groups DOX20). Control mice were injected with an equal volume of saline following the DOX20 administration regime (eight injections) to discard stress changes due to repeated i.p. administrations. After 4 weeks, mice were led ad-libitum until day 44. Echocardiography analyses were performed every week to follow the cardiac dysfunction of mice. Hearts were collected at the end-point of the experiment (day 44). C57BL/6J mice in each experimental condition (n=3). After settling the best model of study, wild-type female C57BL/6J mice (10 weeks old) were randomly assigned into the following 6 groups (n = 6/group): Control, DOX, DOX + Navitoclax, DOX + **GalNP(Nav),** DOX + **Nav-Gal**. Doxorubicin was administered as before, in a chronic regime (cumulative dose, 20 mg/kg, i.p.), in eight equal intraperitoneal injections (2.5 mg/kg) for 4 weeks. Senolytic treatment was administered for 2 consecutive days following DOX administration. Free Navitoclax was formulated in 15% DMSO/ 85% PEG400 (50 mg/kg/day, o.g.) [26], **GalNP(Nav)** was prepared in free-serum DMEM and administered in the maximum tolerated dose (0.8 mg NP/day in 200 µL saline, i.p. equivalent to 0.025 mg Navitoclax/day, i.p), which corresponds with 23x times lower concentration of Navitoclax and **Nav-Gal** was prepared in 10% DMSO/ 90% saline (67 mg/kg/day, i.p., molar equivalent to Navitoclax). An off day was every two cycles. At the end of the experiment, animals were euthanized in a CO_2 atmosphere, and hearts were collected via thoracotomy for *ex vivo* evaluations.

16. Real Time-PCR

The frozen heart samples were used for total RNA extraction. Tissue was disrupted with Trizol according to the manufacturer's instructions (Merck, T9424). The quantities of each total RNA sample were determined using NanoDrop™. Samples were treated with *DNase I* (Nzytech, MB19901) to avoid genomic DNA contamination. The retrotranscription reaction was performed using the PrimeScript RT Reagent Kit (Sumilab, RR037A) following the manufacturer's protocol. qRT-PCR reactions were performed using qPCR Green Master Mix (2x) (Nzytech, MB22402) in a Light Cycler® 480 System (Roche) following the manufacturer's protocol. Data were analyzed using the LightCycler 480 relative quantification software. Nucleotide sequences of the primers used for mRNA expression analyses are listed below:

Table 1. Primer sequences used for qPCR experiments.

Gene	Primer	Sequence (5'→ 3')	GeneBank Number	Size (bp)
p21	Forward	GCAGATCCACAGCGATATCCA	NM_007669.5	73
	Reverse	AACAGGTCGGACATCACCAG		
p53	Forward	TGCATGGACGATCTGTTGCT	NM_011640.3	161
	Reverse	AAAGATGACAGGGGCCATGG		
p16*	Forward	CCCAACGCCCCGAACT	NM_001040654.1	79
	Reverse	GCAGAAGAGCTGCTACGTGAA		
Ccl8	Forward	TAAGGCTCCAGTCACCTGCT	NM_021443.3	119
	Reverse	TCTGGAAAACCACAGCTTCC		
IL-1α	Forward	CGTCAGGCAGAAGTTTGTCA	NM_010554.4	102
	Reverse	TGTTGCAGGTCATTTAACCAA		
TNFα	Forward	ACGGCATGGATCTCAAAGAC	NM_013693.3	116
	Reverse	GTGGGTGAGGAGCACGTAGT		
Sur2a	Forward	CCTTCGGCTCTCGACTTCTA	NM_021041.2	181
	Reverse	ACTCGACCCAAGCAAATTGT		
Nppa*	Forward	ATCTGCCCTCTTGAAAAGCA	NM_008725.3	213
	Reverse	ACACACCACAAGGGCTTAGG		
ActinB	Forward	GTCCACACCCGCCACC	NM_007393.5	168
	Reverse	ACCCATTCCCACCATCACAC		
Gapdh	Forward	TTCACCACCATGGAGAAGGC	NM_001289726.1	52
	Reverse	CCCTTTTGGCTCCACCCT		

*p16 sequence was obtained from [18]. Nppa sequence was obtained from [35].

17. Echocardiography

Parameters of cardiac function were determined using two-dimensional transthoracic echocardiography using a Vivid 7 Pro imaging system (GE Medical Systems). Mice were lightly anesthetized using 1.5% sevoflurane mixed with 100% O_2 during the time of imaging. Echocardiography was performed serially before and during the experimental period. Left ventricular fractional shortening was determined from the M-mode of the parasternal short-axis view by using Vivid Analysis software. All parameters were averaged from at least 3 cardiac cycles per animal at each time point.

18. Immunofluorescence

Collected hearts were washed in PBS, and fixed in 4% PFA for 4h, at room temperature. The fixative was removed and samples were washed in PBS and incubated with 30% sucrose overnight at 4 °C. Fixed tissues were embedded in OCT and frozen completely at −80°C. 7 μm thick heart sections were washed (0.025% Triton X-100 in TBS), then incubated in blocking solution (10% horse serum, 1% BSA, 0.3% Triton X-100, in TBS) for 2 h at room temperature and immunostained following incubation with primary antibody anti-p53 (1:100, Abcam, #ab26) or anti-p21 [HUGO29] (1:75, Abcam, #ab107099) overnight at 4°C (1% BSA, 0.3% Triton X-100, in TBS). Secondary antibodies against mouse or rat conjugated to Alexa Fluor 488/568 (Invitrogen) were used at 1:200 dilutions and incubated for 2h at room temperature and dark. Sections were mounted on microscope slides using the Mowiol/DAPI (Sigma) and covered with a glass coverslip and scanned in a Leica Aperio Versa 200 equipment and quantified with Aperio ImageScope software. Representative images were obtained by using a Leica TCS SP8 HyVolution 2 microscope.

19. Statistical analysis

Statistical analysis of data using GraphPad Prism software 9.0. Comparison of results between groups was made by Student's T-test or One-way ANOVA followed by a Tukey post-test at 95% confidence. A p-value below 0.05 was considered statistically significant (*p<0.05; **p<0.01; ***p<0.001; ****p<0.0001). Data are expressed in more detail for every figure.

Acknowledgments

R.M. laboratory members thank the financial support from the Spanish Government projects RTI2018-100910-B-C41 and RTI2018-101599-B-C22 (MCUI/FEDER, EU)) and the Generalitat Valenciana (project PROMETEO 2018/024). M.O. thanks the financial support from the Spanish Government project (PID2020-115048RB-I00) and the Generalitat Valenciana (project PROMETEO/2019/065). A.L-V. is grateful to the Instituto de Salud Carlos III for her Ph.D. i-PFIS grant (IFI17/00039). A.E-F. and B.L.-T thanks to the Spanish Government for their Ph.D. grant (FPU17/05454) and (FPU15/02707). J.B. thanks to the Instituto de Salud Carlos III for his Sara Borrell contract (CD19/00038). M.A. thanks her postdoctoral fellowship (PAID-10-17). The funders had no role in the design, data collection, decision to publish, or preparation of the manuscript. The authors thank Alberto Hernández for confocal microscopy, Alicia Martínez for flow cytometry, and Laura Ramírez for genomics guidance. The authors thank for the use of Biorender.com.

A.L.-V. performed biological experiments, contributed to the experimental designs, data analysis, discussion, and wrote the manuscript. A. E.-F. contributed to the experimental design, animal experiments, data analysis, and discussion. A.M.-A. and M.A. performed nanoparticle synthesis and characterization. B.L-T. and J.B. performed the prodrug synthesis and characterization. V.B. contributed to animal experiments and echocardiography analysis. A.G.-F. and P.S. contributed to the experimental designs, discussion, and writing. M.O. and R.M.-M. designed and supervised the study. All authors revised and commented on the manuscript.

References

[1] A. Hernandez-Segura, J. Nehme, M. Demaria, Hallmarks of Cellular Senescence, Trends Cell Biol. 28 (2018) 436–453. https://doi.org/10.1016/J.TCB.2018.02.001.

[2] D. Muñoz-Espín, M. Serrano, Cellular senescence: from physiology to pathology, Nat. Rev. Mol. Cell Biol. 2014 157. 15 (2014) 482–496. https://doi.org/10.1038/nrm3823.

[3] B.G. Childs, H. Li, J.M. Van Deursen, Senescent cells: a therapeutic target for cardiovascular disease, J. Clin. Invest. 128 (2018) 1217–1228. https://doi.org/10.1172/JCI95146.

[4] I. Shimizu, T. Minamino, Cellular senescence in cardiac diseases, J. Cardiol. 74 (2019) 313–319. https://doi.org/10.1016/J.JJCC.2019.05.002.

[5] D. Torella, M. Rota, D. Nurzynska, E. Musso, A. Monsen, I. Shiraishi, E. Zias, K. Walsh, A. Rosenzweig, M.A. Sussman, K. Urbanek, B. Nadal-Ginard, J. Kajstura, P. Anversa, A. Leri, Cardiac stem cell and myocyte aging, heart failure, and insulin-like growth factor-1 overexpression, Circ. Res. 94 (2004) 514–524. https://doi.org/10.1161/01.RES.0000117306.10142.50.

[6] R. Anderson, A. Lagnado, D. Maggiorani, A. Walaszczyk, E. Dookun, J. Chapman, J. Birch, H. Salmonowicz, M. Ogrodnik, D. Jurk, C. Proctor, C. Correia-Melo, S. Victorelli, E. Fielder, R. Berlinguer-Palmini, A. Owens, L.C. Greaves, K.L. Kolsky, A. Parini, V. Douin-Echinard, N.K. LeBrasseur, H.M. Arthur, S. Tual-Chalot, M.J. Schafer, C.M. Roos, J.D. Miller, N. Robertson, J. Mann, P.D. Adams, T. Tchkonia, J.L. Kirkland, J. Mialet-Perez, G.D. Richardson, J.F. Passos, Length-independent telomere damage drives post-mitotic cardiomyocyte senescence, EMBO J. 38 (2019). https://doi.org/10.15252/EMBJ.2018100492.

[7] M. Demaria, M.N. O'Leary, J. Chang, L. Shao, S. Liu, F. Alimirah, K. Koenig, C. Le, N. Mitin, A.M. Deal, S. Alston, E.C. Academia, S. Kilmarx, A. Valdovinos, B. Wang, A. De Bruin, B.K. Kennedy, S. Melov, D. Zhou, N.E. Sharpless, H. Muss, J. Campisi, Cellular Senescence Promotes Adverse Effects of Chemotherapy and Cancer Relapse, Cancer Discov. 7 (2017) 165–176. https://doi.org/10.1158/2159-8290.CD-16-0241.

[8] X. Li, M. Liu, R. Sun, Y. Zeng, S. Chen, P. Zhang, Cardiac complications in cancer treatment - A review, Hellenic J. Cardiol. 58 (2017) 190–193. https://doi.org/10.1016/J.HJC.2016.12.003.

[9] Y. Octavia, C.G. Tocchetti, K.L. Gabrielson, S. Janssens, H.J. Crijns, A.L. Moens, Doxorubicin-induced cardiomyopathy: from molecular mechanisms to therapeutic strategies, J. Mol. Cell. Cardiol. 52 (2012) 1213–1225.

https://doi.org/10.1016/J.YJMCC.2012.03.006.

[10] G.H. Oliveira, M.Y. Qattan, S. Al-Kindi, S.J. Park, Advanced heart failure therapies for patients with chemotherapy-induced cardiomyopathy, Circ. Hear. Fail. 7 (2014) 1050–1058. https://doi.org/10.1161/CIRCHEARTFAILURE.114.001292.

[11] Y. Maejima, S. Adachi, H. Ito, K. Hirao, M. Isobe, Induction of premature senescence in cardiomyocytes by doxorubicin as a novel mechanism of myocardial damage, Aging Cell. 7 (2008) 125–136. https://doi.org/10.1111/J.1474-9726.2007.00358.X.

[12] P. Spallarossa, P. Altieri, C. Aloi, S. Garibaldi, C. Barisione, G. Ghigliotti, G. Fugazza, A. Barsotti, C. Brunelli, Doxorubicin induces senescence or apoptosis in rat neonatal cardiomyocytes by regulating the expression levels of the telomere binding factors 1 and 2, Am. J. Physiol. Heart Circ. Physiol. 297 (2009). https://doi.org/10.1152/AJPHEART.00068.2009.

[13] E. Piegari, A. De Angelis, D. Cappetta, R. Russo, G. Esposito, S. Costantino, G. Graiani, C. Frati, L. Prezioso, L. Berrino, K. Urbanek, F. Quaini, F. Rossi, Doxorubicin induces senescence and impairs function of human cardiac progenitor cells, Basic Res. Cardiol. 108 (2013). https://doi.org/10.1007/S00395-013-0334-4.

[14] M.A. Mitry, D. Laurent, B.L. Keith, E. Sira, C.A. Eisenberg, L.M. Eisenberg, S. Joshi, S. Gupte, J.G. Edwards, Accelerated cardiomyocyte senescence contributes to late-onset doxorubicin-induced cardiotoxicity, Am. J. Physiol. Cell Physiol. 318 (2020) C380–C391. https://doi.org/10.1152/AJPCELL.00073.2019.

[15] J. Chang, Y. Wang, L. Shao, R.M. Laberge, M. Demaria, J. Campisi, K. Janakiraman, N.E. Sharpless, S. Ding, W. Feng, Y. Luo, X. Wang, N. Aykin-Burns, K. Krager, U. Ponnappan, M. Hauer-Jensen, A. Meng, D. Zhou, Clearance of senescent cells by ABT263 rejuvenates aged hematopoietic stem cells in mice, Nat. Med. 22 (2016) 78–83. https://doi.org/10.1038/NM.4010.

[16] M.P. Baar, R.M.C. Brandt, D.A. Putavet, J.D.D. Klein, K.W.J. Derks, B.R.M. Bourgeois, S. Stryeck, Y. Rijksen, H. van Willigenburg, D.A. Feijtel, I. van der Pluijm, J. Essers, W.A. van Cappellen, W.F. van IJcken, A.B. Houtsmuller, J. Pothof, R.W.F. de Bruin, T. Madl, J.H.J. Hoeijmakers, J. Campisi, P.L.J. de Keizer, Targeted Apoptosis of Senescent Cells Restores Tissue Homeostasis in Response to Chemotoxicity and Aging, Cell. 169 (2017) 132-147.e16. https://doi.org/10.1016/J.CELL.2017.02.031.

[17] M. Xu, T. Pirtskhalava, J.N. Farr, B.M. Weigand, A.K. Palmer, M.M. Weivoda, C.L. Inman, M.B. Ogrodnik, C.M. Hachfeld, D.G. Fraser, J.L. Onken, K.O. Johnson, G.C.

Verzosa, L.G.P. Langhi, M. Weigl, N. Giorgadze, N.K. LeBrasseur, J.D. Miller, D. Jurk, R.J. Singh, D.B. Allison, K. Ejima, G.B. Hubbard, Y. Ikeno, H. Cubro, V.D. Garovic, X. Hou, S.J. Weroha, P.D. Robbins, L.J. Niedernhofer, S. Khosla, T. Tchkonia, J.L. Kirkland, Senolytics improve physical function and increase lifespan in old age, Nat. Med. 24 (2018) 1246–1256. https://doi.org/10.1038/S41591-018-0092-9.

[18] D.J. Baker, B.G. Childs, M. Durik, M.E. Wijers, C.J. Sieben, J. Zhong, R. A. Saltness, K.B. Jeganathan, G.C. Verzosa, A. Pezeshki, K. Khazaie, J.D. Miller, J.M. Van Deursen, Naturally occurring p16(Ink4a)-positive cells shorten healthy lifespan, Nature. 530 (2016) 184–189. https://doi.org/10.1038/NATURE16932.

[19] A. Hoshino, Y. Mita, Y. Okawa, M. Ariyoshi, E. Iwai-Kanai, T. Ueyama, K. Ikeda, T. Ogata, S. Matoba, Cytosolic p53 inhibits Parkin-mediated mitophagy and promotes mitochondrial dysfunction in the mouse heart, Nat. Commun. 4 (2013). https://doi.org/10.1038/NCOMMS3308.

[20] J.L. Kirkland, T. Tchkonia, Y. Zhu, L.J. Niedernhofer, P.D. Robbins, The Clinical Potential of Senolytic Drugs, J. Am. Geriatr. Soc. 65 (2017) 2297–2301. https://doi.org/10.1111/JGS.14969.

[21] B. Lozano-Torres, A. Estepa-Fernández, M. Rovira, M. Orzáez, M. Serrano, R. Martínez-Máñez, F. Sancenón, The chemistry of senescence, Nat. Rev. Chem. 3 (2019) 426–441. https://doi.org/10.1038/s41570-019-0108-0.

[22] Y. Zhu, T. Tchkonia, H. Fuhrmann-Stroissnigg, H.M. Dai, Y.Y. Ling, M.B. Stout, T. Pirtskhalava, N. Giorgadze, K.O. Johnson, C.B. Giles, J.D. Wren, L.J. Niedernhofer, P.D. Robbins, J.L. Kirkland, Identification of a novel senolytic agent, navitoclax, targeting the Bcl-2 family of anti-apoptotic factors, Aging Cell. 15 (2016) 428–435. https://doi.org/10.1111/acel.12445.

[23] F.C. Lewis-McDougall, P.J. Ruchaya, E. Domenjo-Vila, T. Shin Teoh, L. Prata, B.J. Cottle, J.E. Clark, P.P. Punjabi, W. Awad, D. Torella, T. Tchkonia, J.L. Kirkland, G.M. Ellison-Hughes, Aged-senescent cells contribute to impaired heart regeneration, Aging Cell. 18 (2019). https://doi.org/10.1111/ACEL.12931.

[24] C.A. Schiffer, J.E. Cortes, A. Hochhaus, G. Saglio, P. Le Coutre, K. Porkka, S. Mustjoki, H. Mohamed, N.P. Shah, Lymphocytosis after treatment with dasatinib in chronic myeloid leukemia: Effects on response and toxicity, Cancer. 122 (2016) 1398. https://doi.org/10.1002/CNCR.29933.

[25] A. Walaszczyk, E. Dookun, R. Redgrave, S. Tual-Chalot, S. Victorelli, I. Spyridopoulos, A. Owens, H.M. Arthur, J.F. Passos, G.D. Richardson,

Pharmacological clearance of senescent cells improves survival and recovery in aged mice following acute myocardial infarction, Aging Cell. 18 (2019). https://doi.org/10.1111/ACEL.12945.

[26] E. Dookun, A. Walaszczyk, R. Redgrave, P. Palmowski, S. Tual-Chalot, A. Suwana, J. Chapman, E. Jirkovsky, L. Donastorg Sosa, E. Gill, O.E. Yausep, Y. Santin, J. Mialet-Perez, W. Andrew Owens, D. Grieve, I. Spyridopoulos, M. Taggart, H.M. Arthur, J.F. Passos, G.D. Richardson, Clearance of senescent cells during cardiac ischemia-reperfusion injury improves recovery, Aging Cell. 19 (2020). https://doi.org/10.1111/ACEL.13249.

[27] S. Cang, C. Iragavarapu, J. Savooji, Y. Song, D. Liu, ABT-199 (venetoclax) and BCL-2 inhibitors in clinical development, J. Hematol. Oncol. 8 (2015). https://doi.org/10.1186/S13045-015-0224-3.

[28] W.C. Claycomb, N.A. Lanson, B.S. Stallworth, D.B. Egeland, J.B. Delcarpio, A. Bahinski, N.J. Izzo, HL-1 cells: A cardiac muscle cell line that contracts and retains phenotypic characteristics of the adult cardiomyocyte, Proc. Natl. Acad. Sci. U. S. A. 95 (1998) 2979–2984. https://doi.org/10.1073/PNAS.95.6.2979/ASSET/975EC7AA-E0D3-4238-957F-E3D76AE2BBCB/ASSETS/GRAPHIC/PQ0582673003.JPEG.

[29] X. Yu, J. Zheng, T. Cai, Z. Wang, G. Zhu, Testosterone antagonizes paraquat-induced cardiomyocyte senescence via the mIGF-1/SIRT1 signaling pathway, Brazilian J. Med. Biol. Res. 53 (2020) 1–9. https://doi.org/10.1590/1414-431X20209849.

[30] G.P. Dimri, X. Leet, G. Basile, M. Acosta, G. Scorrt, C. Roskelley, E.E. Medrano, M. Linskensi, I. Rubeljii, O. Pereira-smithii, M. Peacocket, J. Campisi, A biomarker that identifies senescent human cells in culture and in aging skin in vivo, 92 (1995) 9363–9367.

[31] A. Shimizu, J.I. Nishida, Y. Ueoka, K. Kato, T. Hachiya, Y. Kuriaki, N. Wake, CyclinG contributes to G2/M arrest of cells in response to DNA damage, Biochem. Biophys. Res. Commun. 242 (1998) 529–533. https://doi.org/10.1006/BBRC.1997.8004.

[32] B.D. Chang, Y. Xuan, E. V. Broude, H. Zhu, B. Schott, J. Fang, I.B. Roninson, Role of p53 and p21waf1/cip1 in senescence-like terminal proliferation arrest induced in human tumor cells by chemotherapeutic drugs, Oncogene. 18 (1999) 4808–4818. https://doi.org/10.1038/SJ.ONC.1203078.

[33] A. Chicas, X. Wang, C. Zhang, M. McCurrach, Z. Zhao, O. Mert, R.A. Dickins, M. Narita, M. Zhang, S.W. Lowe, Dissecting the unique role of the retinoblastoma tumor

suppressor during cellular senescence, Cancer Cell. 17 (2010) 376–387. https://doi.org/10.1016/J.CCR.2010.01.023.

[34] A. Agostini, L. Mondragõn, A. Bernardos, R. Martínez-Máñez, M. Dolores Marcos, F. Sancenõn, J. Soto, A. Costero, C. Manguan-García, R. Perona, M. Moreno-Torres, R. Aparicio-Sanchis, J.R. Murguía, Targeted cargo delivery in senescent cells using capped mesoporous silica nanoparticles, Angew. Chem. Int. Ed. Engl. 51 (2012) 10556–10560. https://doi.org/10.1002/ANIE.201204663.

[35] D. Muñoz-Espín, M. Rovira, I. Galiana, C. Giménez, B. Lozano-Torres, M. Paez-Ribes, S. Llanos, S. Chaib, M. Muñoz-Martín, A.C. Ucero, G. Garaulet, F. Mulero, S.G. Dann, T. VanArsdale, D.J. Shields, A. Bernardos, J.R. Murguía, R. Martínez-Máñez, M. Serrano, A versatile drug delivery system targeting senescent cells, EMBO Mol. Med. 10 (2018). https://doi.org/10.15252/EMMM.201809355.

[36] I. Galiana, B. Lozano-Torres, M. Sancho, M. Alfonso, A. Bernardos, V. Bisbal, M. Serrano, R. Martínez-Máñez, M. Orzáez, Preclinical antitumor efficacy of senescence-inducing chemotherapy combined with a nanoSenolytic, J. Control. Release. 323 (2020) 624–634. https://doi.org/10.1016/J.JCONREL.2020.04.045.

[37] A. Estepa-Fernández, M. Alfonso, Á. Morellá-Aucejo, A. García-Fernández, A. Lérida-Viso, B. Lozano-Torres, I. Galiana, P.M. Soriano-Teruel, F. Sancenón, M. Orzáez, R. Martínez-Máñez, Senolysis Reduces Senescence in Veins and Cancer Cell Migration, Adv. Ther. 2100149 (2021) 1–15. https://doi.org/10.1002/adtp.202100149.

[38] E. González-Gualda, M. Pàez-Ribes, B. Lozano-Torres, D. Macias, J.R. Wilson, C. González-López, H.L. Ou, S. Mirón-Barroso, Z. Zhang, A. Lérida-Viso, J.F. Blandez, A. Bernardos, F. Sancenón, M. Rovira, L. Fruk, C.P. Martins, M. Serrano, G.J. Doherty, R. Martínez-Máñez, D. Muñoz-Espín, Galacto-conjugation of Navitoclax as an efficient strategy to increase senolytic specificity and reduce platelet toxicity, Aging Cell. 19 (2020). https://doi.org/10.1111/ACEL.13142.

[39] B. Meiners, C. Shenoy, B.N. Zordoky, Clinical and preclinical evidence of sex-related differences in anthracycline-induced cardiotoxicity, Biol. Sex Differ. 9 (2018) 38. https://doi.org/10.1186/s13293-018-0198-2.

[40] C.J. Zeiss, D.M. Gatti, O. Toro-Salazar, C. Davis, C.M. Lutz, F. Spinale, T. Stearns, M.B. Furtado, G.A. Churchill, Doxorubicin-Induced Cardiotoxicity in Collaborative Cross (CC) Mice Recapitulates Individual Cardiotoxicity in Humans, G3 Genes|Genomes|Genetics. 9 (2019) 2637–2646. https://doi.org/10.1534/G3.119.400232.

[41] S.E. Lipshultz, E.H. Herman, Anthracycline cardiotoxicity: the importance of horizontally integrating pre-clinical and clinical research, Cardiovasc. Res. 114 (2018) 205–209. https://doi.org/10.1093/CVR/CVX246.

[42] A.D. Hudgins, C. Tazearslan, A. Tare, Y. Zhu, D. Huffman, Y. Suh, Age- and Tissue-Specific Expression of Senescence Biomarkers in Mice, Front. Genet. 9 (2018). https://doi.org/10.3389/FGENE.2018.00059.

[43] M.S. Chen, R.T. Lee, J.C. Garbern, Senescence mechanisms and targets in the heart, Cardiovasc. Res. 118 (2022) 1173. https://doi.org/10.1093/CVR/CVAB161.

[44] S. Gallo, M. Spilinga, R. Albano, G. Ferrauto, E. Di Gregorio, E. Casanova, D. Balmativola, A. Bonzano, C. Boccaccio, A. Sapino, P.M. Comoglio, T. Crepaldi, Activation of the MET receptor attenuates doxorubicin-induced cardiotoxicity in vivo and in vitro, Br. J. Pharmacol. 177 (2020) 3107. https://doi.org/10.1111/BPH.15039.

[45] M. Zhao, X. feng Ding, J. yu Shen, X. ping Zhang, X. wen Ding, B. Xu, Use of liposomal doxorubicin for adjuvant chemotherapy of breast cancer in clinical practice, J. Zhejiang Univ. Sci. B. 18 (2017) 15–26. https://doi.org/10.1631/JZUS.B1600303.

[46] P.S. Rawat, A. Jaiswal, A. Khurana, J.S. Bhatti, U. Navik, Doxorubicin-induced cardiotoxicity: An update on the molecular mechanism and novel therapeutic strategies for effective management, Biomed. Pharmacother. 139 (2021). https://doi.org/10.1016/J.BIOPHA.2021.111708.

[47] T. Šimůnek, M. Štěrba, O. Popelová, M. Adamcová, R. Hrdina, V. Gerši, Anthracycline-induced cardiotoxicity: overview of studies examining the roles of oxidative stress and free cellular iron, Pharmacol. Rep. 61 (2009) 154–171. https://doi.org/10.1016/S1734-1140(09)70018-0.

[48] K.N. Timm, C. Perera, V. Ball, J.A. Henry, J.J. Miller, M. Kerr, J.A. West, E. Sharma, J. Broxholme, A. Logan, D. Savic, M.S. Dodd, J.L. Griffin, M.P. Murphy, L.C. Heather, D.J. Tyler, Early detection of doxorubicin-induced cardiotoxicity in rats by its cardiac metabolic signature assessed with hyperpolarized MRI, Commun. Biol. 3 (2020) 1–10. https://doi.org/10.1038/s42003-020-01440-z.

[49] S. Häseli, S. Deubel, T. Jung, T. Grune, C. Ott, Cardiomyocyte Contractility and Autophagy in a Premature Senescence Model of Cardiac Aging, Oxid. Med. Cell. Longev. 2020 (2020). https://doi.org/10.1155/2020/8141307.

[50] J. Shi, P.W. Kantoff, R. Wooster, O.C. Farokhzad, Cancer nanomedicine: progress, challenges and opportunities, Nat. Rev. Cancer. 17 (2017) 20–37. https://doi.org/10.1038/NRC.2016.108.

[51] G.C. Meléndez, S. Vasu, E.J. Lesnefsky, J.R. Kaplan, S. Appt, R.B. D'Agostino, W.G. Hundley, J.H. Jordan, Myocardial Extracellular and Cardiomyocyte Volume Expand After Doxorubicin Treatment Similar to Adjuvant Breast Cancer Therapy, JACC. Cardiovasc. Imaging. 13 (2020) 1084–1085. https://doi.org/10.1016/J.JCMG.2019.10.020.

[52] T.I. Janjua, Y. Cao, C. Yu, A. Popat, Clinical translation of silica nanoparticles, Nat. Rev. Mater. 2021 612. 6 (2021) 1072–1074. https://doi.org/10.1038/s41578-021-00385-x.

[53] K. Bukara, L. Schueller, J. Rosier, M.A. Martens, T. Daems, L. Verheyden, S. Eelen, M. Van Speybroeck, C. Libanati, J.A. Martens, G. Van Den Mooter, F. Frérart, K. Jolling, M. De Gieter, B. Bugarski, F. Kiekens, Ordered mesoporous silica to enhance the bioavailability of poorly water-soluble drugs: Proof of concept in man, Eur. J. Pharm. Biopharm. 108 (2016) 220–225. https://doi.org/10.1016/j.ejpb.2016.08.020.

[54] J. Zhao, H. Fuhrmann-Stroissnigg, A.U. Gurkar, R.R. Flores, A. Dorronsoro, D.B. Stolz, C.M. St. Croix, L.J. Niedernhofer, P.D. Robbins, Quantitative Analysis of Cellular Senescence in Culture and In Vivo, Curr. Protoc. Cytom. 79 (2017) 9.51.1-9.51.25. https://doi.org/10.1002/CPCY.16.

Supporting Information

Pharmacological senolysis reduces doxorubicin-induced cardiotoxicity and improves cardiac function in mice

Araceli Lérida-Viso[1,2,3,4], Alejandra Estepa- Fernández[2,3,4], Ángela Morellá-Aucejo[2,3,4], Beatriz Lozano-Torres[2,3,4], María Alfonso[2], Juan F. Blandez[1,2,4], Viviana Bisbal[5], Pilar Sepúlveda[6,7], Alba García-Fernández[2,3,4,*], Mar Orzáez[3,5,*], Ramón Martínez-Máñez[1,2,3,4,*].

1 Unidad Mixta de Investigación en Nanomedicina y Sensores. Universitat Politècnica de València (UPV)- Instituto de Investigación Sanitaria La Fe (IIS La Fe).
Av. Fernando Abril Martorell 106, Valencia 46026, Spain

2 Instituto Interuniversitario de Investigación de Reconocimiento Molecular y Desarrollo Tecnológico (IDM). Universitat Politècnica de València.
Camino de Vera, s/n, Valencia 46022, Spain

3 Unidad Mixta UPV-CIPF de Investigación en Mecanismos de Enfermedades y Nanomedicina. Universitat Politècnica de València-Centro de Investigación Príncipe Felipe.
C/ Eduardo Primo Yúfera 3, Valencia 46012, Spain

4 CIBER de Bioingeniería Biomateriales y Nanomedicina (CIBER-BBN).

5 Centro de Investigación Príncipe Felipe.
C/ Eduardo Primo Yúfera 3, Valencia 46012, Spain.

6 Regenerative Medicine and Heart Transplantation Unit. Instituto de Investigación Sanitaria La Fe. Av. Fernando Abril Martorell 106, Valencia 46026, Spain

7 CIBER de Enfermedades Cardiovasculares (CIBERCV).

E-mail: algarfe4@etsia.upv.es; morzaez@cipf.es; rmaez@qim.upv.es

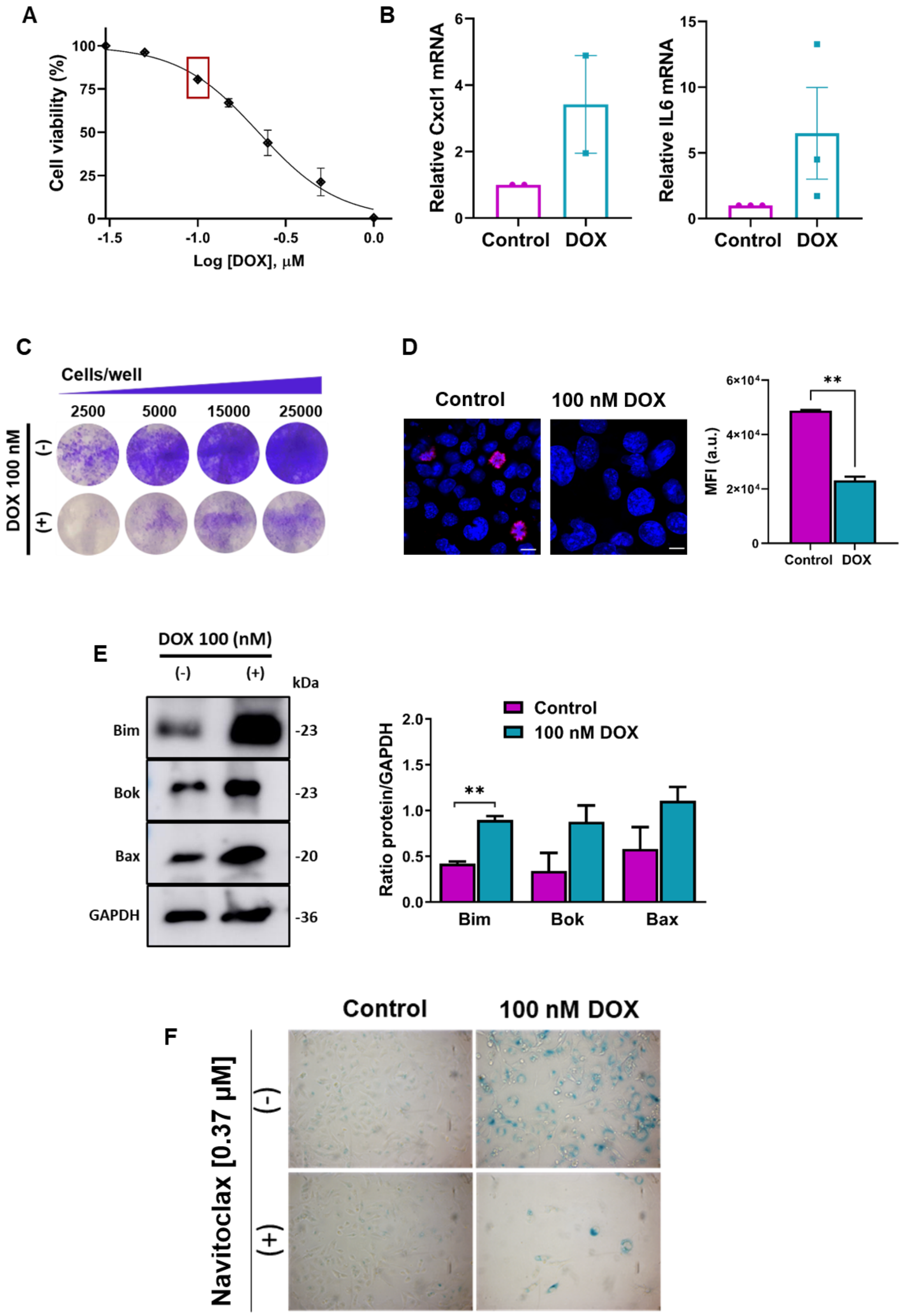

Figure S1. (A) Dose-response curve of DOX in HL-1 cells incubated with the indicated range of drug concentrations for 3 days (0 to 1 μM). Data shown are mean effect relative to vehicle-only control wells ± SEM (n=3). Red square indicates 100 nM DOX. (**B**) mRNA expression levels of the SASP makers, *Cxcl1* and *IL6*, in control and DOX-treated HL-1 cells. SASP markers are overexpressed in DOX-treated cells, *Actb* was used for input normalization. Values are relative to control cells and are expressed as mean ± SEM ($n \geq 2$). (**C**) Cell proliferation arrest assay by crystal violet staining. The same number of control and DOX-treated cells were seeded increasing cell number (2500; 5000; 15000; 25000) in a 24-well plate and were let to proliferate for one week. Cell cycle arrest was confirmed by crystal violet staining. (**D**) (Left) Representative images of immunofluorescence of Ki67 (red fluorescence) in control and DOX-treated HL-1 cells by confocal microscopy. The nucleus is stained with Hoechst 33342 (blue). The expression of the cell proliferation marker Ki67 decreases upon senescence induction with DOX. Scale bar, 10 μm. (Right) Quantification of mean fluorescence intensity of Ki67 red signal corresponding to 3 different fields. Bars represent the mean ± SEM and statistical significance was assessed by the two-tailed Student's t-test: $^{**}p < 0.01$. (**E**) Western blot analysis expression showing increased expression of pro-apoptotic members Bim (23 kDa), Bok (23 kDa), and Bax (20 kDa) were found in DOX-treated HL-1 cells. GAPDH (37 kDa) determination was included as a loading control. (Right) Quantification of the ratio of pro-apoptotic protein expression versus internal control (GAPDH) in control and DOX-treated cells. Values are expressed as mean ± SEM and statistical significance was assessed by the two-tailed Student's t-test: $^{**}p < 0.01$ (n=3). (**F)** Representative bright-field images of SA-β-gal staining of control and 100 nM DOX-treated HL-1 cells non-treated (upper panels) or Navitoclax treated for 48h (bottom panels) at IC50 concentration for senescent cells (0.37 μM). Blue staining confirms high β-galactosidase activity DOX treatment. Navitoclax exposure resulted in a reduction in the number of senescent cells but not control, which reinforces the role of Navitoclax as a senolytic therapy.

A Senescent protein profile

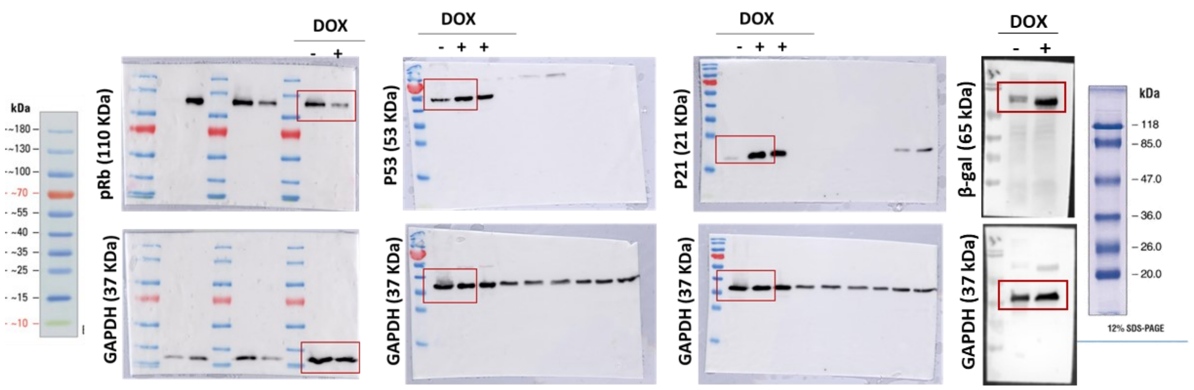

B Bcl2 family protein profile

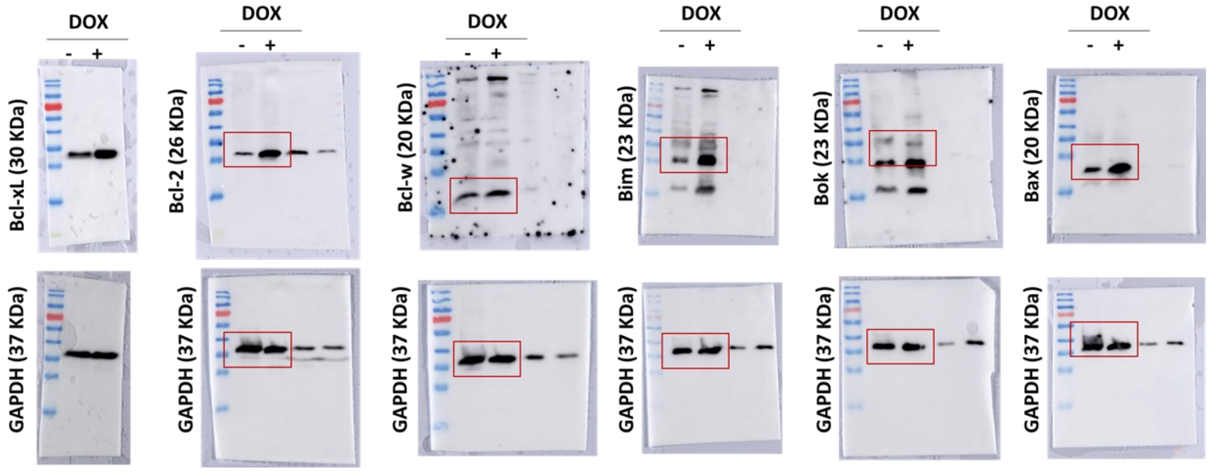

Figure S2. Original western blots images. (A) Senescent proteins expression in control and DOX-treated HL-1 cells. **(B)** Blc2 family protein profile in control and DOX-treated HL-1 cells. GAPDH (37 kDa) determination was included as a loading control.

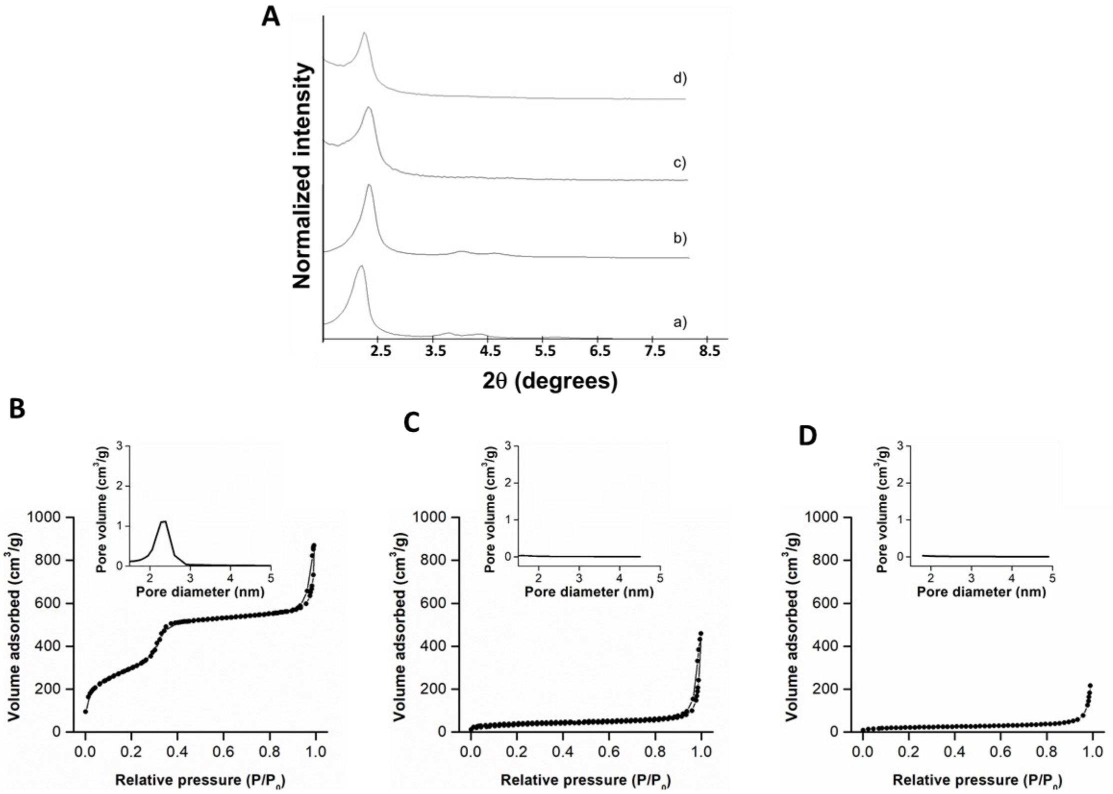

Figure S3. Characterization of synthesis of nanoparticulated systems. (A) Powder X-Ray diffraction patterns at low (left) and high (right) angles of (a) **starting MSNs** (b) **calcined MSNs**, (c) **GalNP(ICG)**, and (d) **GalNP**. N_2 adsorption-desorption isotherms for **(B) calcined MSNs**, **(C) (GalNP(ICG),** and **(D) GalNP**.

Table S1. BET specific surface values, pore volumes, and pore sizes calculated from N_2 adsorption-desorption isotherms for indicated solids

Solid	SBET $[m^2g^{-1}]$	Pore Volume $[cm^3g^{-1}]$	Pore Size [nm]
Calcined MSNs	1228.80	0.93	3.18
GalNP	55.82	0.12	--
GalNP(ICG)	101.41	0.05	--

Table S2. Hydrodynamic diameter and zeta potential of indicated solids.

Solid	Hydrodynamic particle diameter (nm)	Zeta Potential (mV)
Calcined MSNs	153.5 ± 4.0	-27.1 ± 0.5
GalNP	273.3 ± 3.9	0.03 ± 0.03
GalNP(ICG)	244.5 ± 4.1	-0.06 ± 0.04
GalNP(Nav)	284.8 ± 2.5	0.34 ± 0.02

Table S3. The organic content of molecular gate oligosaccharide, and cargo for nanodevices **GalNP(ICG)** and **GalNP(Nav)** in mg per g of solid.

Solid	$\alpha_{oligosaccharide}$ (mg/g solid)	α_{cargo} (mg/g solid)
GalNP(ICG)	100.7	43
GalNP(Nav)	167.7	54

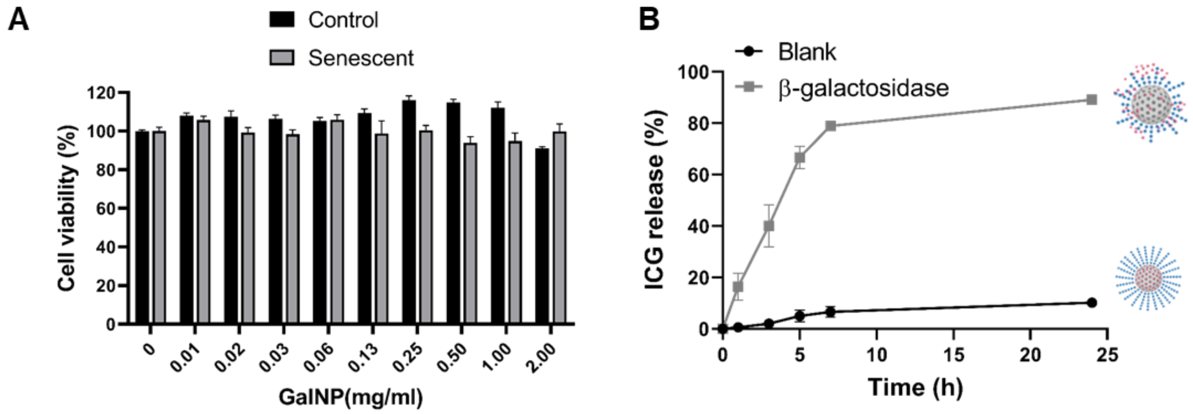

Figure S4. (A) Cell viability of control and senescent HL-1 cells after treatment with **GalNP** at increasing concentrations (0-2 mg/ml, filtered) for 72h. **(B)** Release profiles of ICG from **GalNP(ICG)** in the absence (blank) or the presence of β -galactosidase from *Aspergillus oryzae* in water at pH 4.5. Data represent the means ± SEM (n=3).

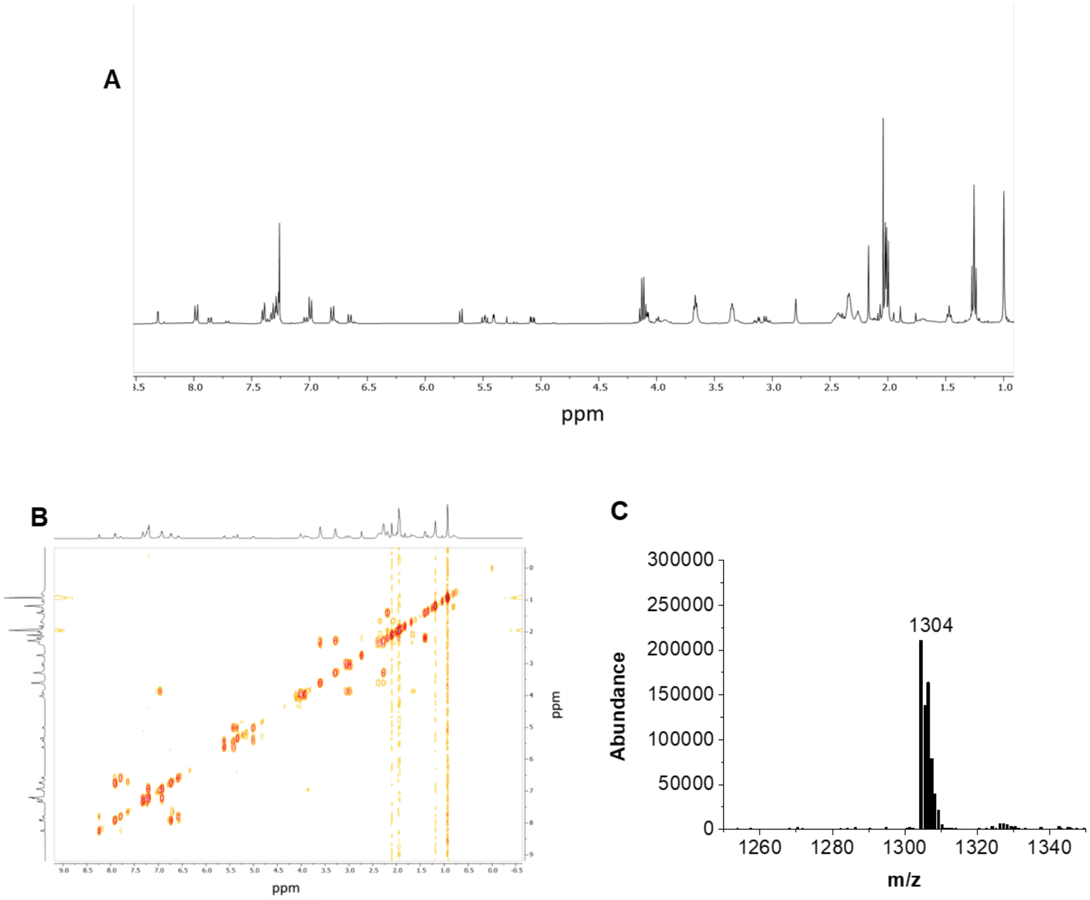

Figure S5. Molecular characterisation of Nav-Gal. (A) Chemical shifts of the signals of protons of Nav-Gal ^{1}H NMR (400 MHz, CDCl3) δ 8.31 (d, J = 2.3 Hz, 1H), 7.98 (d, J = 9.1 Hz, 2H), 7.86 (dd, J = 9.1, 2.3 Hz, 1H), 7.41-7.26 (m, 5H), 7.04 6.97 (m, 4H), 6.80 (d, J = 9.3 Hz, 2H), 6.65 (d, J = 9.4 Hz, 1H), 5.69 (d, J = 8.2 Hz, 1H), 5.49 (dd, J = 10.4, 8.2 Hz, 1H), 5.41 (dd, J = 3.5, 1.1 Hz, 1H), 5.07 (dd, J = 10.4, 3.4 Hz, 1H), 4.08 (dd, J = 6.7, 4.7 Hz, 2H), 4.00 (dd, J = 6.5, 1.2 Hz, 1H), 3.70-3.60 (m, 4H), 3.39-3.32 (m, 4H), 3.19 – 3.00 (m, 3H), 2.80 (bs, 2H), 2.50-2.22 (m., 12H), 2.17 (s, 3H), 2.02 (s, 3H), 2.01 (s, 3H), 2.00 (s, 3H), 1.87 (bs, 2H), 1.77 – 1.65 (m, 2H), 1.47 (t, J = 6.4 Hz, 3H), 1.00 (s, 6H). (**B**) Homonuclear bidimensional correlated spectroscopy 1H-1H (2D) COSY NMR (400 MHz, CD3Cl), signals outside of the diagonal arises from the protons that are coupled together in neighboring carbons. (**C**) HRMS of Nav-Gal, molecular ion (M) m/z theorical value calculated 1303, m/z, observed correspond with M+H with a m/z value of 1304.

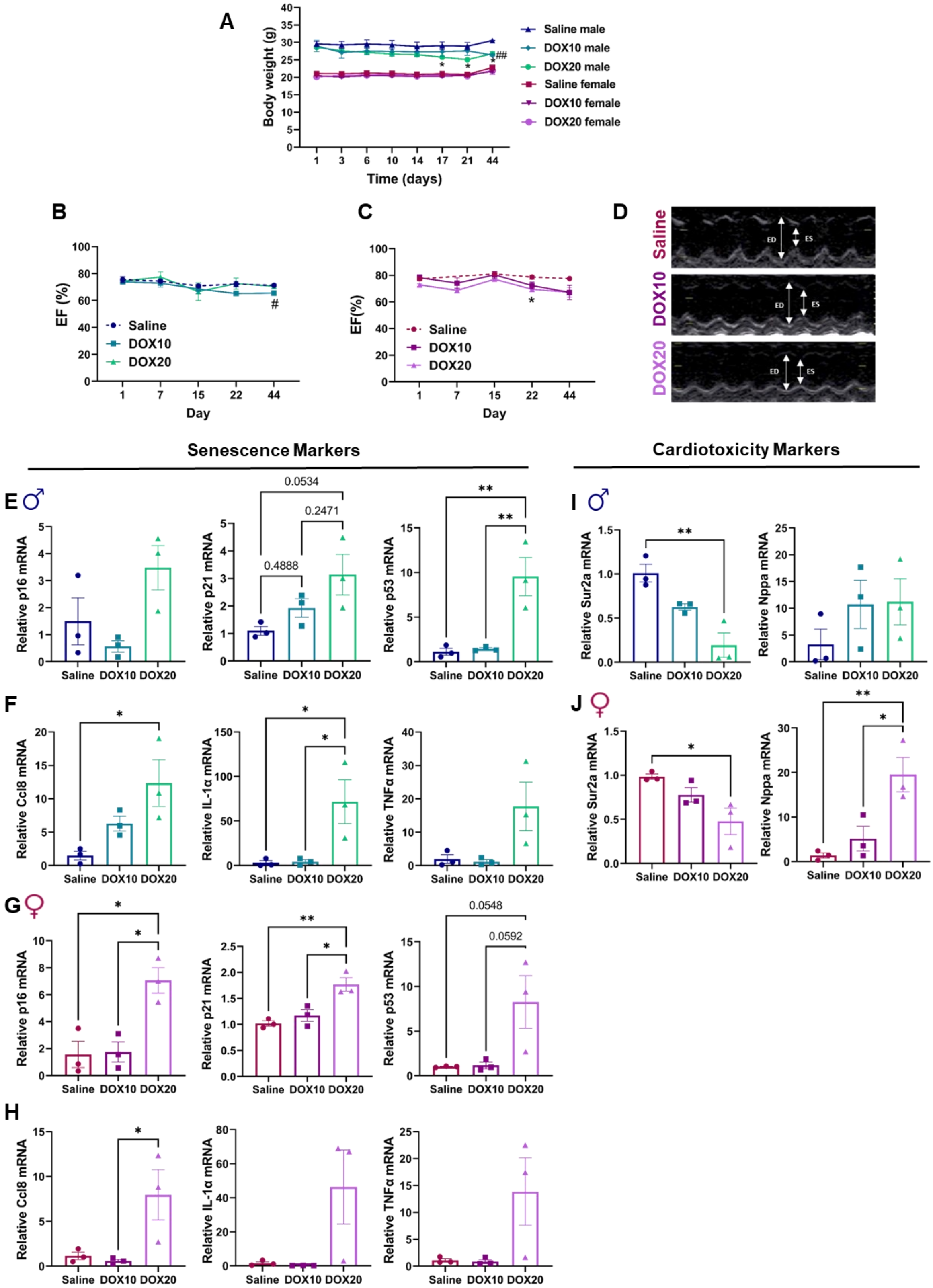

Figure S6. (A) Body weight of male (blue tones) and female (violet tones) mice during 44 days of the experiment. Loss of weight was observed for males treated with DOX from day 17. Non-changes were observed in female mice. Values are expressed as mean ± SEM (n=3). Statistical significance was assessed by the two-tailed Student's t-test: *p < 0.05 (DOX20 vs saline); ## p

< 0.001 (DOX10 vs saline). (**B-C**) Changes in ejection fraction (EF) in male (**B**) and female (**C**) mice during the curse of the experimental. Data represent means ± SEM. Mean of 3 different independent measures is represented for each animal (n=3). Statistical significance was determined by one-way ANOVA and Tukey post-test; #$p < 0.05$ (DOX10 vs Saline-group, for male) and *$p < 0.05$ (DOX20 vs Saline-group, for female). **(D)** Representative echocardiographic analysis of female mice in each experimental condition displaying changes in LV fractional shortening at day 22. (ED= end diastole, ES= end systole). After injection with DOX, a decrease in LV contraction is observed. **(E-J)** mRNA expression levels of the senescent makers, *p16*, *p21*, and *p53*, and in heart tissue of mice; (**E**) for male, (**G**) for female mice. mRNA expression levels of the SASP markers, *Ccl8, IL-1α*, and *TNFα* in heart tissue of mice; (**F**) for male, (**H**) for female mice. mRNA expression levels of cardiotoxicity markers, *Sur2a* and *Nppa*, in heart tissue of mice; (**I**) for male, (**J**) for female mice. *Actb* and *Gapdh* were used for input normalization. Values are relative to control mice and are expressed as mean ± SEM. Statistical significance was determined by one-way ANOVA and Tukey post-test; *$p < 0.05$; **$p < 0.01$ (n=3, heart per group).

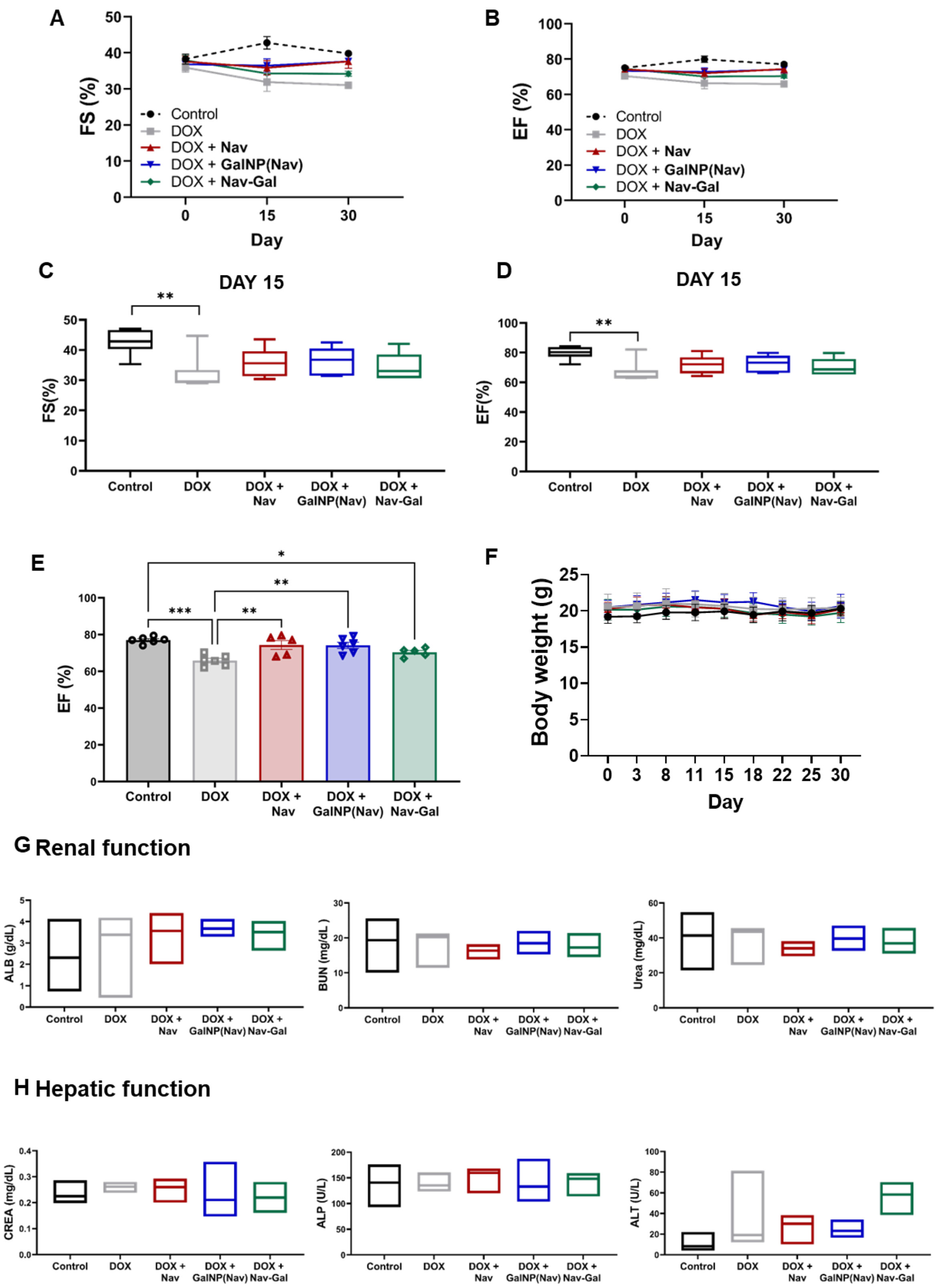

Figure S7. (A-B) Changes in fractional shortening (FS) (**A**) and ejection fraction (EF) (**B**) in mice during the curse of the experimental. Data represent means ± SEM. Mean of 3 different independent measures is represented for each animal (n≥5). (**C-D**) Graphs indicating values of FS (**C**) and EF (**D**) at day 15 for all experimental groups. At this point, a significant decrease in FS and EF values was observed for DOX-treated mice. (**E**) Ejection fraction (EF) values obtained for animals at the experimental end-point (day 30). A decrease in EF value was observed for animals in the DOX group and EF increased upon administration of senolytic treatment. Data represent means of 3 different independent measures for each animal ± SEM ($n \geq 5$). Statistical significance was determined by one-way ANOVA and Tukey post-test; *$p < 0.05$; **$p < 0.01$; ***$p < 0.001$. **(F)** Bodyweight mice during 30 days of experimental. Non-changes were observed in any experimental group. **(G-H)** Analysis of renal (**G**) and hepatic (**H**) function of mice at the end of the treatment. ALB, albumin; BUN, blood urea nitrogen; Urea; CREA, creatinin; ALP, alkaline phosphatase; ALT, alanine transaminase.